FULL CRITICAL REVIEW

Microstructural evolution and high temperature failure of ferritic to austenitic dissimilar welds

J. N. DuPont*

Dissimilar metal welds between ferritic and austenitic alloys are used extensively in power plants. Premature failure of such welds can occur below the expected creep life of either base metal. This article reviews microstructural evolution in dissimilar welds and describes factors that contribute to premature failure. The microstructure in the as welded condition consists of a sharp chemical concentration gradient across the fusion line. Martensite forms within this gradient due to high hardenability and rapid cooling rates from welding. Upon aging, carbon diffuses down the chemical potential gradient from the ferritic steel toward the austenitic alloy. This can lead to formation of a soft carbon denuded zone in the ferritic steel, and nucleation and growth of carbides in the austenitic steel that produce high hardness. These differences in microstructure and hardness occur over distances of about 50–100 μm. Failure is attributed to the steep microstructural and mechanical property gradients, the large difference in coefficient of thermal expansion, formation of interfacial carbides that promote creep cavity formation, and preferential oxidation of the ferritic steel. Information is also provided on available creep rupture properties, remaining life estimation techniques, current best practices and research in progress.

1 **Keywords:** Dissimilar metal welds, Creep failure

Introduction

Dissimilar metal welds (DMWs) between ferritic low alloy steels and austenitic alloys are commonly used in fossil and nuclear power plants. The less expensive low alloy steels are used in the low temperature regions of the plant, while the higher temperature regions require the superior corrosion resistance and greater creep strength of more expensive austenitic alloys. There can be thousands of DMWs in a single plant. Experience to date has demonstrated that failures of DMWs can occur prematurely at service times below the expected creep life of either base metal and well below the design life of the plant. The failure time depends on a wide range of factors related to service conditions, welding parameters, and alloys involved in the DMW. The failures can generally be attributed to large differences in chemical composition, coefficient of thermal expansion (CTE), and creep strength between the two alloys. Premature failure can result in forced plant outages that can cost a power company up to $850 000/day in lost revenue.[1] Several important changes have been made in the design and fabrication procedures of DMWs that significantly improve service life. These include improved weld designs and selection of better filler metals along with the use of transition joints that help reduce CTE mismatch. However, failures still often occur in unacceptable time frames and can have a serious impact on plant efficiency and availability.

The problem of premature DMW failures will continue to be a concern in the future due to two factors. First, many existing plants are nearing or have past their original design life. The large cost associated with construction of new plants has resulted in life extension programs that will push the operation of many plants well beyond their original design life. This will require life extension of existing DMWs, as well as installation of new DMWs as older joints fail and require replacement. In addition, new fossil and nuclear plants are being designed to operate at higher temperatures and pressures for improved efficiency. The improved efficiency is driven by the need to conserve fuel sources and minimise environmental impact. In terms of fossil fired plants, new designs in so called ultrasupercritical plants are being considered that will operate at elevated steam temperatures and pressures of 760°C and 35 MPa respectively.[2] The US Department of Energy is also funding research and development of a new nuclear plant that involves the use of a high temperature gas cooled reactor[3] that operates at higher temperatures than those currently in the USA. In the proposed system, alloy 800H is expected to be used for the superheater section, and 2·25Cr–1Mo steel is expected to be used for the evaporator–economiser

Department of Materials Science and Engineering, Lehigh University, Bethlehem, PA, USA

*Corresponding author, email jnd1@lehigh.edu

© 2012 Institute of Materials, Minerals and Mining and ASM International
Published by Maney for the Institute and ASM International
Received 20 June 2011; accepted 5 March 2012
DOI 10.1179/1743280412Y.0000000006

International Materials Reviews imr199.3d 28/3/12 16:41:00
The Charlesworth Group, Wakefield +44(0)1924 369598 - Rev 7.51n/W (Jan 20 2003)

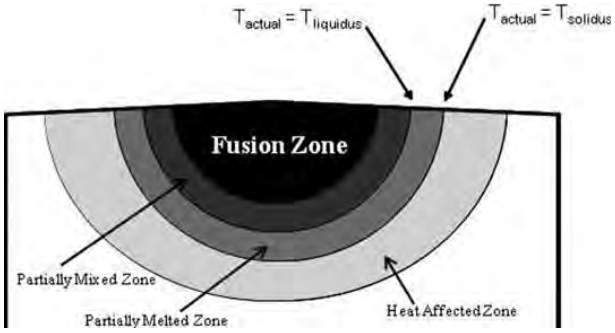

1 Schematic illustration of four distinct microstructural zones that exist in dissimilar welds

section. Dissimilar metal welds will be needed to join these two materials. Thus, considering these factors, there is still considerable interest in understanding the factors associated with DMW failures and developing techniques for improving their performance.

The overall objective of this article is to review factors associated with premature failure of DMWs operating at elevated temperatures and identify methods for extending their life. The review focuses primarily on welds involving 2·25Cr–1Mo steel as the ferritic component, since these joints are of primary importance for a large range of applications. Both iron base stainless steels and nickel base alloys are considered, since both have been used as the austenitic component of DMWs. It should be noted, however, that the majority of concepts are broadly applicable to a wide range of ferritic to austenitic dissimilar alloy combinations. The review begins with a description of microstructural evolution that occurs around the interface between ferritic and austenitic materials in both the as welded and aged conditions. The failure mechanism of DMWs operating at high temperatures is then reviewed, followed by an assessment of the creep rupture behaviour of DMWs relative to 2·25Cr–1Mo steel base metal and welds. The effect of aging on the mechanical properties of the filler metal that is most commonly used for DMWs is also considered. Techniques for remaining life assessment are then discussed. The review concludes with a description of research currently in progress for improving the performance of DMWs and suggestions for future research.

Microstructural evolution

As welded condition

Welds made between two dissimilar alloys will generally consist of four distinct microstructural zones as shown schematically in Fig. 1. The fusion zone is the region where complete mixing occurs between the two base metals and (if used) the filler metal. There is considerable fluid flow that occurs in the weld metal, while in the liquid state that is driven by a variety of sources, including differences in density and surface tension along with impingement from the high temperature plasma.[4] Thus, the composition within the fusion zone is generally macroscopically uniform due to this rather aggressive mixing that occurs before solidification. However, within the fusion zone, there is a stagnant boundary layer near the partially melted base metal where mixing between the base metal and filler metal is incomplete. A partially mixed zone (PMZ) forms in this

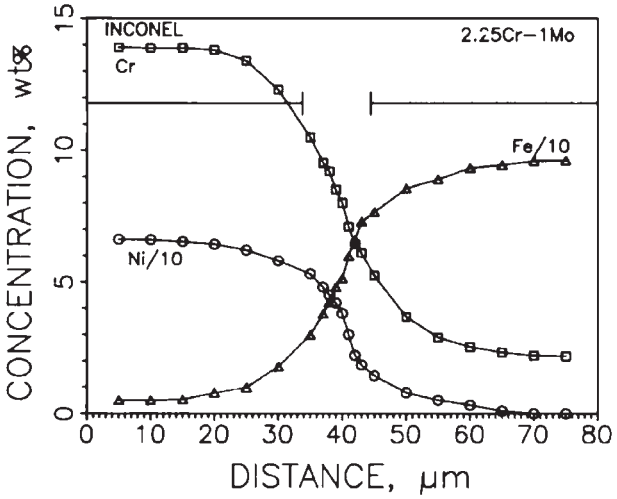

2 Distribution of major alloying elements in PMZ of dissimilar weld between 2·25Cr–1Mo and alloy 800H: zero point in figure is arbitrary

small region in which the composition gradually changes from that of the fusion zone to that of the base metal. The composition gradients associated with the PMZs of DMWs are particularly important in terms of microstructural evolution and resultant service performance. They are discussed in more detail below. Near the PMZ will be a region where the actual temperature during welding was between the liquidus and solidus of the base. This region will exhibit various degrees of liquation that can often be observed microstructurally (e.g. localised melting of secondary phases), but the composition in this region is identical to the base metal, since no mixing occurred with the filler metal. The heat affected zone (HAZ) consists of the region within the base metal where the actual temperature is below the terminal solidus temperature of the alloy, but above the temperature at which solid state transformations will occur.

The distribution of major alloying elements in the PMZ of a dissimilar weld between 2·25Cr–1Mo and alloy 800H is shown in Fig. 2[5] as an example. This weld was fabricated using the shielded metal arc welding process with Inconel 182 electrode. The chemical compositions of typical high temperature materials discussed in this review are provided in Table 1. The region of partial mixing that occurred before solidification is clearly observed as a transition in composition between the 2·25Cr–1Mo base metal and the fusion zone. Similar composition profiles are available in the literature for a wide range of dissimilar alloy combinations[6–8] and demonstrate that a PMZ of finite width always forms, regardless of the alloys involved and welding parameters utilised. The actual width of the PMZ depends on welding variables such as heat input and filler metal feed rate.[7] Under most welding conditions, the size of the PMZ is very small (<100 μm) in relation to the width of the fusion zone. However, PMZs as large as 2–3 mm have been observed under very high filler metal feed rate conditions.[7]

As shown by Fig. 2, the Ni content in the PMZ will decrease from the fusion zone toward the low alloy steel

Table 1 Chemical compositions of typical high temperature materials (wt-%)

International Materials Reviews imr199.3d 28/3/12 16:41:02
The Charlesworth Group, Wakefield +44(0)1924 369598 - Rev 7.51n/W (Jan 20 2003)

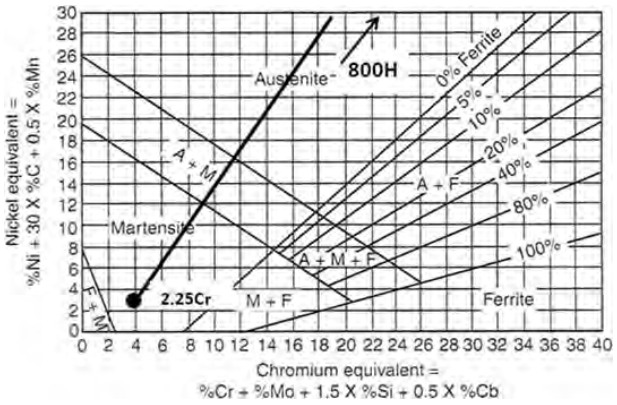

3 Schaeffler diagram used for prediction of microstructure in ferritic, austenitic and dissimilar welds: line on figure represents change in composition within PMZ for weld made between alloy 800 and 2·25Cr–1Mo steel; note that composition of alloy 800 is outside diagram

base metal. A point will eventually be reached where the Ni content is too low to stabilise the austenite during cooling to room temperature. In addition, the relatively high alloy content within this zone promotes high hardenability. As a result, martensite will form under even the slowest cooling rate conditions associated with fusion welding. This can be understood with reference to the Schaeffler diagram shown in Fig. 3.[4] This diagram reveals the microstructural constituents that form in welds of alloy steels and stainless steels under cooling rate conditions typical of arc welding. Use of the diagram is appropriate for interpreting microstructural formation in the PMZ of dissimilar welds, since the composition in this zone falls within the experimentally verified regions of the diagram. This is shown in Fig. 3 by plotting the Ni and Cr equivalents for alloy 800H and 2·25Cr–1Mo steel directly on the Schaeffler diagram. Since the PMZ will consist of all compositions that connect these two points, the PMZ has to traverse through a martensitic region. Similar results are expected and have been verified for DMWs made between other steels and austenitic alloys (i.e. stainless steels and nickel base alloys).[6,8,9]

Examples of the martensite layers that form within the PMZ of dissimilar welds between ferritic steel and stainless steel, as well as ferritic steel and Ni base alloy are shown in Fig. 4.[6] As shown by the photomicrographs in Fig. 4, the use of Ni base filler metals will result in the formation of a thin martensite layer at the fusion line, while the martensite layer that results from the use of stainless steel filler metals is relatively thick. Recent work[6] has shown that this difference is attributed to the variations in concentration gradients that exist in the PMZ between the two types of filler metal. The black vertical line in each photomicrograph of Fig. 4 represents the locations of composition traces acquired with electron probe microanalysis. The variation in martensite layer widths is readily evident from these figures. The martensite layer in the 309L weld was 30–37 μm in thickness, while that in the IN625 weld was only 1–3 μm in thickness.

The variation in major alloying elements (Fe, Ni and Cr) across the fusion lines of the welds is shown in Fig. 5. The composition gradient is steeper for the weld prepared with IN625 filler metal, because of the increase in nominal Ni content and decrease in nominal Fe content compared to the weld prepared with 309L stainless steel. The composition gradients produce a variation in the martensite start temperature M_s across the fusion line, and the differences in composition gradients and resultant M_s gradients between the two welds can be used to explain the observed variation in martensite widths. Using the measured values for Ni, Cr and Mo along with estimated values of C and Mn, the variation in M_s across the PMZ was determined. Figure 6 shows the results of M_s calculated from the composition profiles according to the expression provided by Gooch [6] in which M_s (°C)= 540–497%C + 6·3%Mn + 36·3%Ni + 10·8%Cr + 46·6%Mo (all values in weight per cent). The two curves on each plot represent the highest and lowest possible M_s based on the range in dilution that was experimentally determined within the PMZ. The martensite layer within the PMZ should begin near the start of the composition gradient near the carbon steel base metal and end at a location where the M_s intersects room temperature. The exact start and end locations cannot be known with a high degree of certainty, since this will depend on the local hardenability (as determined by local composition) and local cooling rate. However, comparison of the M_s gradient plots in Fig. 6 clearly shows that a thinner martensite layer is expected in welds prepared with Ni base filler metals. This can be attributed to the higher concentration gradient within the PMZ (due to higher Ni concentration), which, in turn, 4

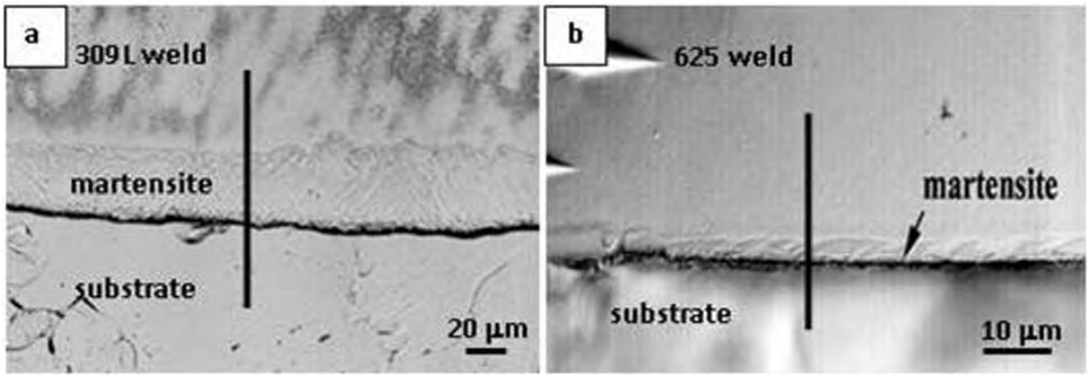

4 Light optical photomicrographs showing examples of martensite layers that form within PMZ in dissimilar welds between ferritic steel and *a* 309L stainless steel filler metal and *b* alloy 625 filler metal: samples were electrolytically etched using 90 mL methanol/5 g FeCl/4 mL HCl solution

International Materials Reviews imr199.3d 28/3/12 16:41:04
The Charlesworth Group, Wakefield +44(0)1924 369598 - Rev 7.51n/W (Jan 20 2003)

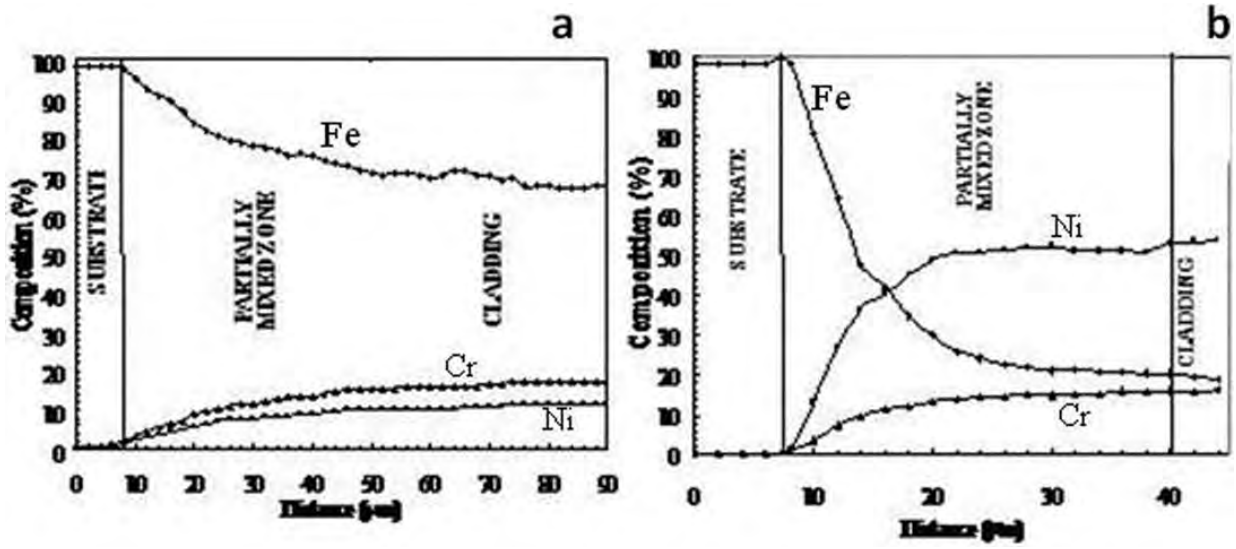

a weld between ferritic steel and 309L stainless steel filler metal; *b* weld between ferritic steel and alloy 625 filler metal

5 Variation in major alloying elements (Fe, Ni and Cr) across fusion lines of welds shown in Fig. 4

stabilises the austenite at a shorter location from the fusion line within the PMZ.

According to Fig. 6, the martensite layer should be approximately 35–39 μm for the weld prepared with 309L filler metal and approximately 2–3 μm in the weld prepared with the IN625 filler metal. These values compare reasonably well with those measured at the location of the microprobe trace for each weld in Fig. 4, ~34 μm for 309L and ~3 μm for IN625. It should be noted that the exact width of the martensite layer can vary within a given weld due to local variations in the composition gradient (due to local variations in fluid flow behaviour) and local differences in cooling rate. In addition, variations in fluid flow behaviour are expected when changes are made to processing parameters. The objective of the results presented here is not to predict the size of the martensite layer within a given weld or with variations in processing parameters, but to demonstrate why significant differences exist between the widths of martensite layers in welds prepared with Ni base and Fe base alloys.

Figure 7 illustrates the large differences in hardness that develop near the interface in DMWs.[9] The example shown is for a DMW between 2·25Cr–1Mo steel and a 309L stainless steel, but similar trends have been observed for welds made between many other weld combinations. Note that the hardness in the 2·25Cr–1Mo steel decreases from ~300 to 227 HV near the fusion line. The slight reduction in hardness is attributed to carbon diffusion from the high C ferritic steel to the low C stainless steel and is discussed in more detail in the next section. This effect can be observed microstructurally in Fig. 7, since there is less carbide (dark etching constituent) near the interface where the C content and associated hardness are low. There is then a large increase in hardness to 435 HV over a very short distance, and the high hardness is associated with formation of the martensite layer. It has recently been suggested[10] that martensite formation can be avoided in DMWs by careful control over the welding parameters so that the cooling rate is low enough to avoid martensite formation within the concentration gradient of the PMZ. Unfortunately, no detailed microstructural information was provided to support this claim, and this is not consistent with the large body of experimental evidence[5,6,9,11–16] that clearly shows that martensite will always form under the combination of composition and cooling rate associated with practical welding conditions.

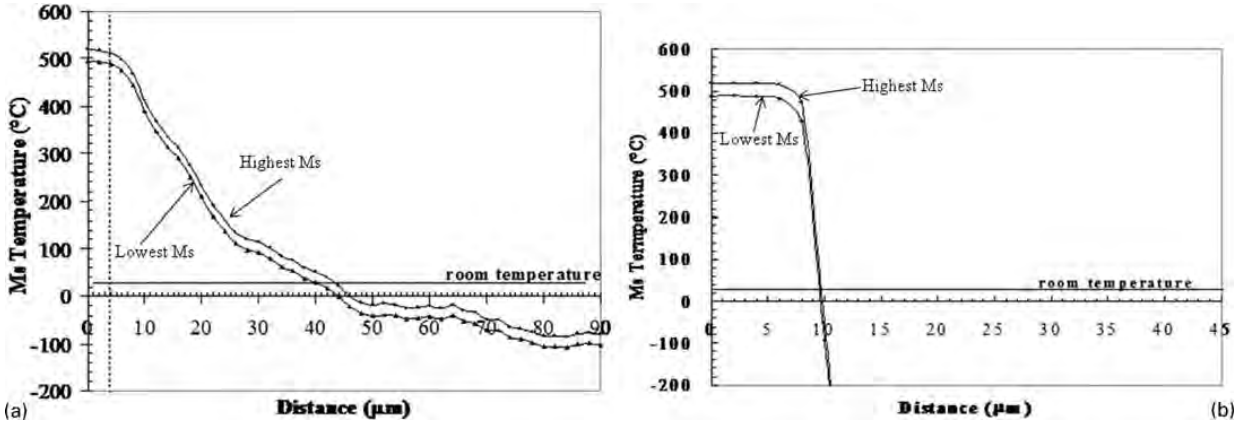

6 Variation in martensite start temperature M_s across PMZ for *a* weld between ferritic steel and 309L stainless steel filler metal and *b* weld between ferritic steel and alloy 625 filler metal: martensite start temperatures were calculated based on composition: equation used to calculate M_s are referenced in text

International Materials Reviews imr199.3d 28/3/12 16:41:09
The Charlesworth Group, Wakefield +44(0)1924 369598 - Rev 7.51n/W (Jan 20 2003)

ONLINE COLOUR ONLY

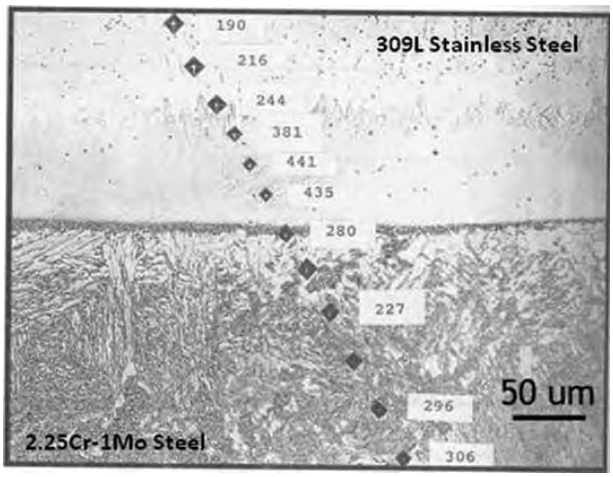

7 Differences in hardness that develop in as welded condition near interface for weld between 2·25Cr–1Mo steel and 309L stainless steel

Microstructural evolution during aging and post-weld heat treatment (PWHT)

The concentration gradient within the PMZ, together with large differences in C solubility and diffusivity between the ferritic and austenitic alloys, leads to significant microstructural changes during PWHT and aging in service. Figure 8 shows the microstructure and hardness variations that exist in DMWs involving 2·25Cr–1Mo steel with stainless steel and Ni base filler metals after a PWHT is applied.[9] Figure 7 (as welded condition) can be compared directly with Fig. 8 (PWHT condition), since these figures are from the same study. Note that the hardness differences are now pronounced even further, with the minimum hardness of the 2·25Cr–1Mo steel decreased to 134 HV (compared to 227 HV in the as welded condition) and the maximum hardness in the PMZ increased to 487 (compared to 441 HV in the as welded condition). The hardness gradient for the weld made with the Ni based filler metal appears to be smaller compared to that observed for the weld made with the stainless steel filler metal. This trend has been observed by several investigators and reported to be a potential advantage of Ni base filler metals.[11–13,17] However, as discussed above, welds made with Ni base filler metals exhibit sharper concentration gradients than those prepared with stainless steel filler metals. As discussed in more detail below, the large differences in hardness are associated with a thin layer of carbides that precipitate within the concentration gradient. The carbide layer is expected to be very thin when the concentration gradient is steep, and the microhardness measurements may not have sufficient resolution to detect the locally high hardness associated with the thin carbide layer that forms in welds made with Ni base filler metals. Note that a dark etching band also appears at the end of the PMZ after application of a PWHT.

Measurements of C concentration profiles within the PMZ are difficult due to its low atomic number and low concentration. However, it is readily evident that the C concentration profile in the as welded condition will look similar to that of Fe shown in Fig. 2, since the C content of the ferritic steel is typically higher than that of the austenitic alloy. Thus, there is a C concentration gradient that is high in the ferritic alloy and decreases toward the austenitic alloy. At elevated temperatures, C will diffuse down the chemical potential gradient. In view of this, it is important to note that Cr lowers the chemical potential of C,[5,18] and the Cr level increases from the ferritic side to the austenitic side of the interface. Thus, the C and Cr concentration gradients produce a rather sharp C chemical potential gradient across the interface. Furthermore, the diffusivity of C in ferrite is significantly higher than in austenite, and the solubility is significantly lower. As a result of these factors, there is a strong driving force for C to diffuse from the ferritic alloy to the austenitic alloy. This produces a decarburised layer in the ferritic side that accounts for the significant reduction in hardness. Carbon migration has been shown to be an important component of DMW failures and has received much attention in the literature.[18–23] This is discussed in more detail in a later section.

Note from Fig. 7 that some decarburisation can also occur during the welding operation. Although C diffusion also occurs in welds made with Ni base alloys, the problem is substantially reduced to the point where a decarburised layer is very small or not observed at all on the ferritic side of the joint.[9,11,13,24,25] Carbon diffusion towards the austenitic alloy side of the joint also leads to a C enriched region just inside the fusion line. An example of this is shown from examination of a service exposed weld in Fig. 9.[17] Just beyond the interface, on the austenitic side of the fusion line, the C concentration is significantly enriched to the point where the solubility limit of C in austenite is exceeded. This leads to formation of carbides within this region. Transmission electron

ONLINE COLOUR ONLY

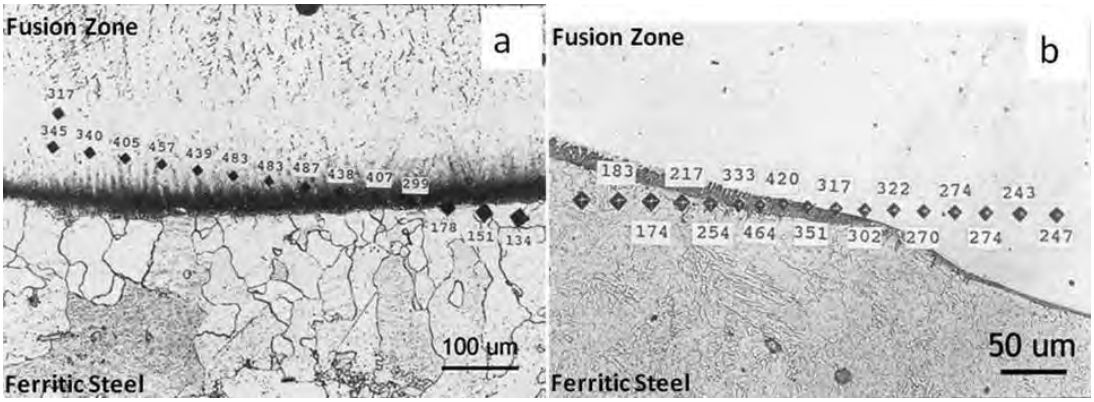

8 Microstructure and hardness variations that exist in weld involving 2·25Cr–1Mo steel with *a* 309 stainless steel after PWHT of 720°C for 10 h and *b* ERNiCr-3 filler metal after PWHT of 690°C for 30 h

International Materials Reviews imr199.3d 28/3/12 16:41:19
The Charlesworth Group, Wakefield +44(0)1924 369598 - Rev 7.51n/W (Jan 20 2003)

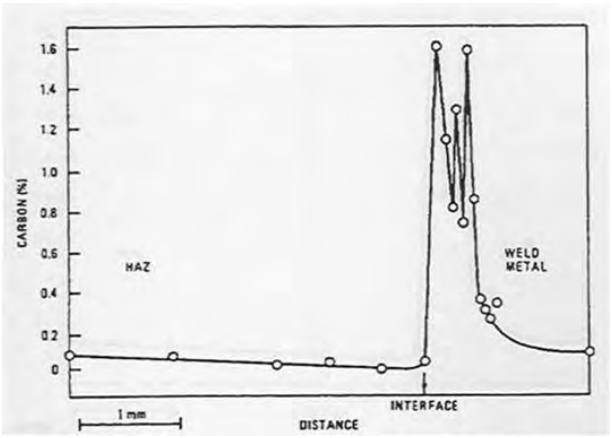

9 Carbon concentration profile across fusion line of service exposed weld made on reheater piping (operating at 540–565°C) with 2·25Cr–1Mo steel and Inconel filler metal

micrographs of carbon replicas showing an example the carbides that form in this zone are provided in Fig. 10.[9] Detailed microstructural characterisation studies[9,26–28] have shown that these are $M_{23}C_6$ and M_6C carbides.

Figure 11[5] shows the variations in microhardness across the interfacial region of a weld made between 2·25Cr–1Mo steel and alloy 800H in the as welded condition, after application of a PWHT at 700°C for 1 h, and after creep testing at 150 MPa/550°C (with a corresponding failure time of approximately 1000 h). This weld was made with Inconel 182 filler metal. The interface position is noted in the figure. The high hardness in the 2·25Cr–1Mo steel HAZ directly after welding is attributed to formation of martensite in this region. Note that the HAZ hardness is decreased considerably after PWHT. However, a highly localised hardness peak evolves just inside the interface on the fusion zone side of the weld, and this peak hardness increases after creep testing. The localised increase in hardness that occurs with increased aging time is associated with nucleation and growth of the carbides in the PMZ that occurs due to

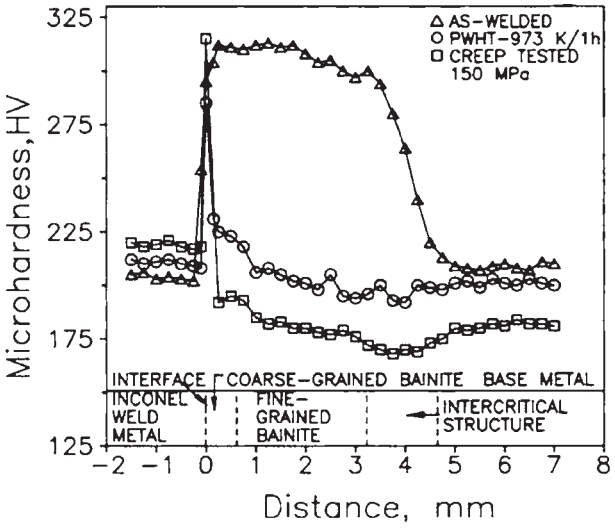

11 Variations in microhardness across interfacial region of weld made between 2·25Cr–1Mo steel and alloy 800H in as welded condition, after application of PWHT at 700°C for 1 h, and after creep testing at 150 MPa/550°C (with corresponding failure time of ~1000 h)

C diffusion. Figure 12 compares hardness differences in welds involving 2·25Cr–1Mo steel with Inconel 182 filler metal (Fig. 12*a*) and 316 stainless steel filer metal (Fig. 12*b*).[29] Results are shown for the PWHT condition (700°C/3 h) and after aging at 580°C. The expected hardness peaks just inside the interface are observed. However, note that the weld made with the 316 stainless steel filler metal also shows a significant decrease in hardness on the 2·25Cr–1Mo side of the weld. Such a hardness trough is not observed in the weld made with the Inconel 182 filler metal.

Gittos and Gooch[9] have demonstrated that the application of a PWHT can also cause increases in hardness due to formation of virgin martensite on cooling from the PWHT temperature. This can be understood with reference to Fig. 13, which shows the variation in composition in the as welded and PWHT condition. The

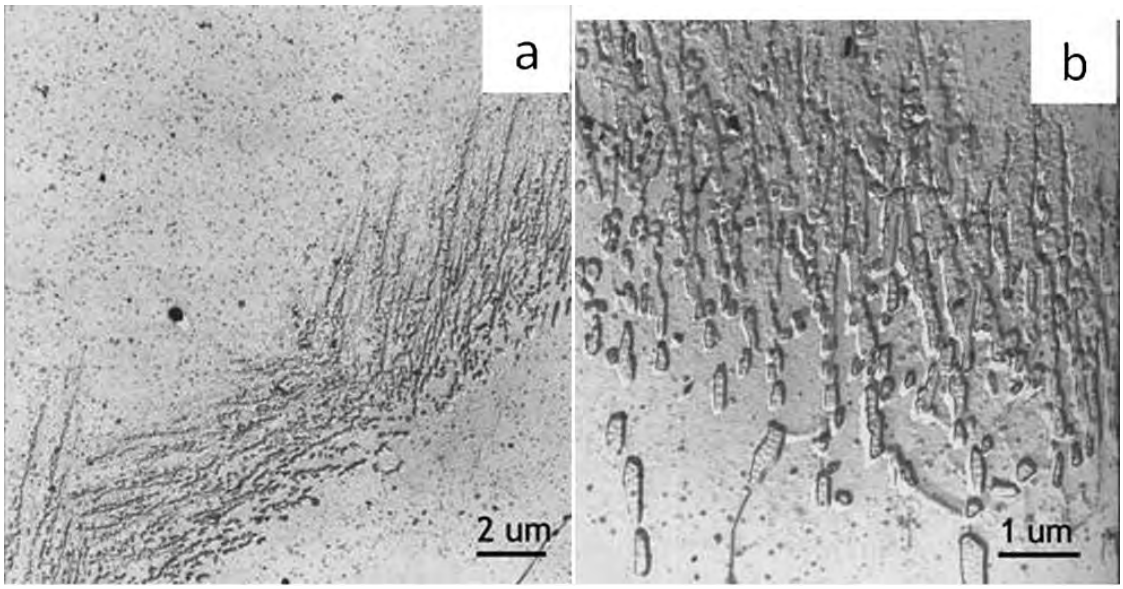

ONLINE COLOUR ONLY

10 Transmission electron micrographs of carbon replicas showing carbides that form in weld between 2·25Cr–1Mo steel and 309 stainless steel after PWHT of 690°C for 30 h

International Materials Reviews imr199.3d 28/3/12 16:41:24
The Charlesworth Group, Wakefield +44(0)1924 369598 - Rev 7.51n/W (Jan 20 2003)

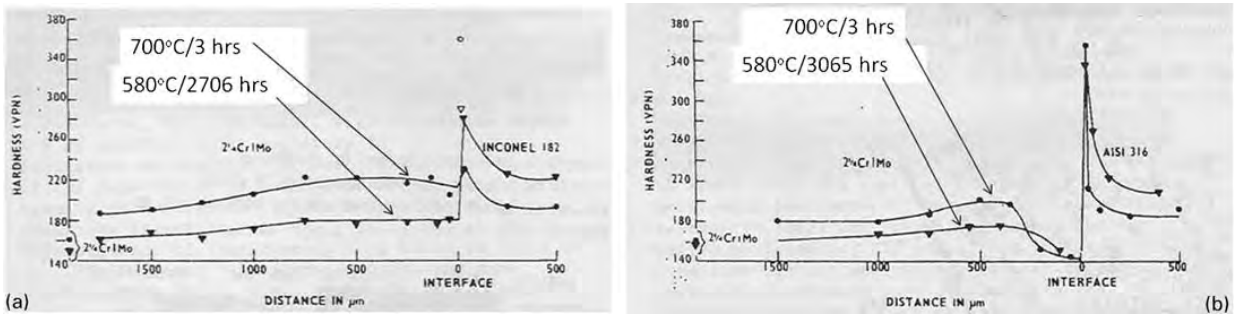

12 Microhardness profiles in welds involving 2·25Cr–1Mo steel with *a* Inconel 182 filler metal and *b* 316 stainless steel filler metal after PWHT at 700°C for 3 h and after aging at 580°C

diffusion rates of substitutional alloying elements are generally too low to promote composition changes during PWHT and aging.[30] Thus, the C content is the only one which will change near the interface after exposure to high temperatures at times typical of PWHT. M_s is also shown at several locations within the transition region for the as welded and PWHT condition. These values were estimated from the measured composition gradient. Also noted is the approximate position at which the Ac_1 (i.e. temperature at which ferrite transforms to austenite on heating) is 550°C. This figure is not meant to be exact, but to provide a general description of how the concentration gradient and C migration affect the transformation temperatures. The Ac_1 temperature generally decreases with increasing alloying additions. Thus, as shown in Fig. 13, for most PWHT temperatures (which are approximately 600–700°C), a portion of the PMZ will be re-austenitised during the PWHT, because the Ac_1 is lower than the PWHT temperature. Furthermore, C migration will lead to extensive formation of Cr rich carbides, which reduces the amount of Cr in solution. This raises M_s within this region and also causes virgin martensite to form on cooling from the PWHT.

It is now recognised[12,13,17,31–33] that two distinct carbide morphologies will evolve in DMWs during aging. Examples of these are shown in Fig. 14 for IN182 filler metal used to join 2·25Cr–1Mo steel to 316 stainless steel. Type I carbides (Fig. 14*a* and *b*) are the ones most frequently observed. These form very close to the fusion line (~1 μm) in the HAZ of the ferritic steel. These carbides initially form with a spherical shape, but gradually acquire a lenticular morphology and can eventually form regions of continuous or semicontinuous carbides as they grow and coalesce. Examples of this morphological change are shown by the photomicrographs in Fig. 14*a* (aged at 625°C for 2000 h) and Fig. 14*b* (aged at 625°C for 6000 h). The type II carbides (Fig. 14*c*) generally form as a wide band and are associated with the martensite region that forms within the PMZ.

As discussed in more detail in the next section, examinations of service and laboratory induced failures[12,13,17,31–34] have shown that premature failure of DMWs made with Ni base filler metals is associated with formation of creep cavities around the type I carbides. Thus, the nucleation, growth and morphological changes that occur in type I carbides have received considerable attention, and several kinetic studies have been reported.[14,35,36] Most recently, Parker and Stratford provided a detailed study of the growth rate and change in morphology of type I carbides that occur in the transition region between 2·25Cr–1Mo steel and Inconel 182 filler metal.[17] The carbide sizes and number densities 5

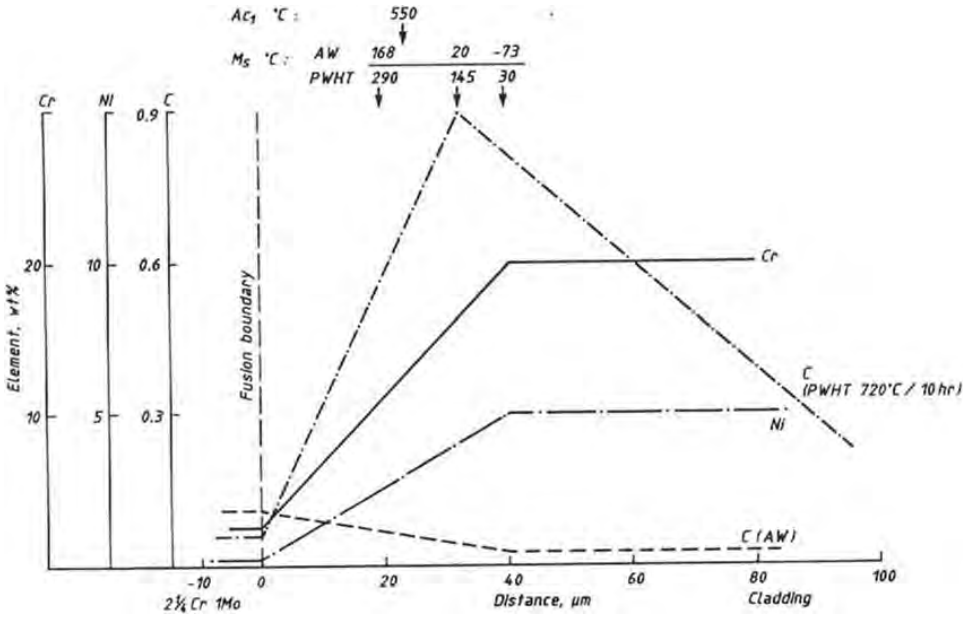

13 Schematic illustration of variation in composition in as welded (AW) and PWHT condition for cladding between 2·25Cr–1Mo steel and 309L stainless steel

International Materials Reviews imr199.3d 28/3/12 16:41:30
The Charlesworth Group, Wakefield +44(0)1924 369598 - Rev 7.51n/W (Jan 20 2003)

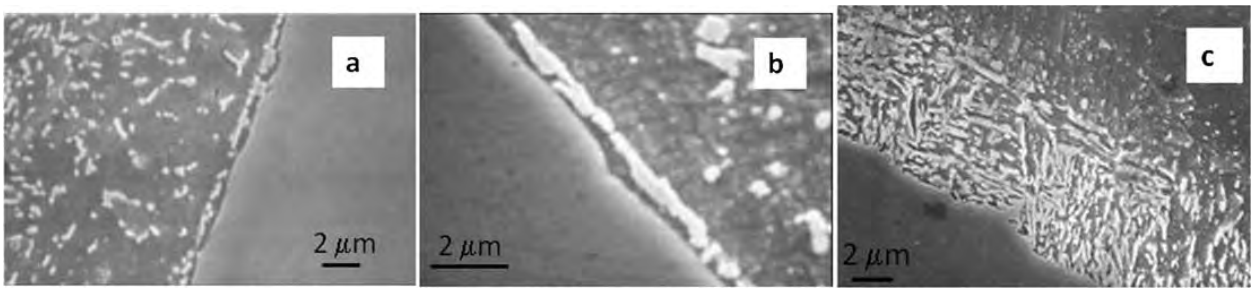

a type I carbides that form very close to fusion line in HAZ of ferritic steel after 2000 h at 625°C; *b* type I carbides that form very close to fusion line in HAZ of ferritic steel after 6000 h at 625°C; *c* type II carbides that form as wide band associated with martensite region

14 Carbide morphologies observed in dissimilar weld during aging for IN182 filler metal used to join 2·25Cr–1Mo steel to 316 stainless steel

were determined on samples aged at 625°C for times up to 6000 h. Samples that were creep tested at temperatures of 590, 605 and 625°C for times between 350 and 8600 h were also included in the study. Figure 15 demonstrates how the major and minor axes of the carbides change with aging time at 625°C. Note that the growth rate of the major axis is higher than that of the minor axis, which supports the view that the carbides become elongated during aging and align themselves along the interface direction (see Fig. 14*a* and *b*). Figure 16 shows the variation in carbide density as measured by number of carbides per unit length. Note that the carbide density increases up to ~2000 h. After this point, the carbides begin to coalesce due to continued growth, often resulting in a continuous or semicontinuous carbide network along the interface. It was also noted that the type II carbides generally dissolved with increased aging time. The data in Fig. 15 for aged (i.e. stress free) and creep tested samples are essentially indistinguishable. Thus, the application of a stress does not appear to affect the growth rate of the carbides.

The change in carbide growth dimensions with time and temperature can be described using the well known Wagner–Lifshitz expression[37,38]

$$D^3 = D_o^3 + Bt \tag{1}$$

where D is the carbide diameter after some exposure time, D_o is the original carbide diameter, B is a temperature dependent material constant and t is time. Since the initial carbide size is small, and taking the temperature dependence of B into account, the carbide diameter can be expressed as

$$D^3 = kt \exp\left(\frac{-Q}{RT}\right) \tag{2}$$

where k is a material constant and Q is the activation energy for growth. Experimentally determined values for Q were developed for both the major (Q=279 kJ mol^{-1}) and minor (Q=257 kJ mol^{-1}) carbide axes.[14] These values compare well with similar results obtained by Viswanathan *et al.*[36] that were acquired on service exposed samples. Nicholson proposed a somewhat similar approach,[35] except he assumed that the carbide particles remained spherical during growth. As a result, his analysis generally underestimates the particle sizes when compared to data obtained from service exposed samples.

The general evolution of microstructure in ferritic to austenitic DMWs is summarised schematically in Figs. 17 and 18 for the as welded and aged condition. In the as welded condition (Fig. 17), there is a sharp concentration gradient within the PMZ that creates a zone of high alloy content (relative to the low alloy steel) and high hardenability. As a result, as quenched martensite forms within the PMZ during cooling from the weld thermal cycle. As quenched martensite also forms in the HAZ of the low alloy steel. The regions of as quenched martensite produce high hardness, but this hardness decreases sharply near the interface between

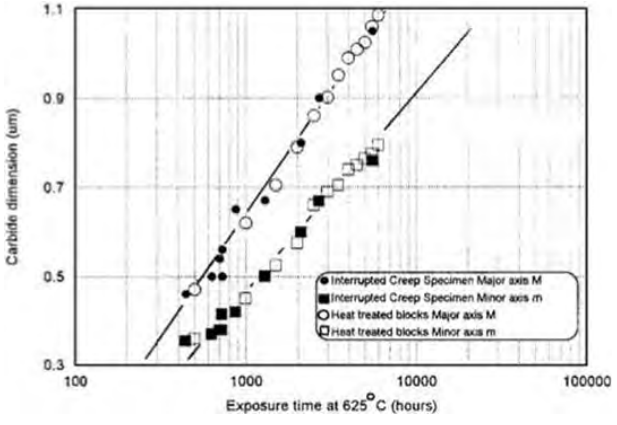

15 Variation in major and minor axes of type I carbides with aging time at 625°C for weld between 2·25Cr–1Mo steel and Inconel 182 filler metal

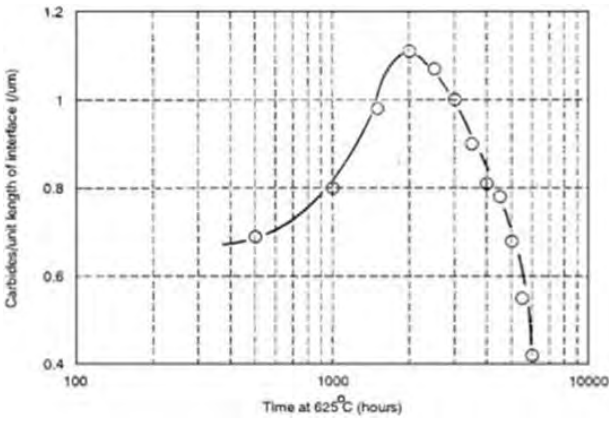

16 Variation in carbide density with aging time at 625°C as measured by number of carbides per unit length for welds between 2·25Cr–1Mo steel and Inconel 182 filler metal

International Materials Reviews imr199.3d 28/3/12 16:41:40
The Charlesworth Group, Wakefield +44(0)1924 369598 - Rev 7.51n/W (Jan 20 2003)

ONLINE COLOUR ONLY

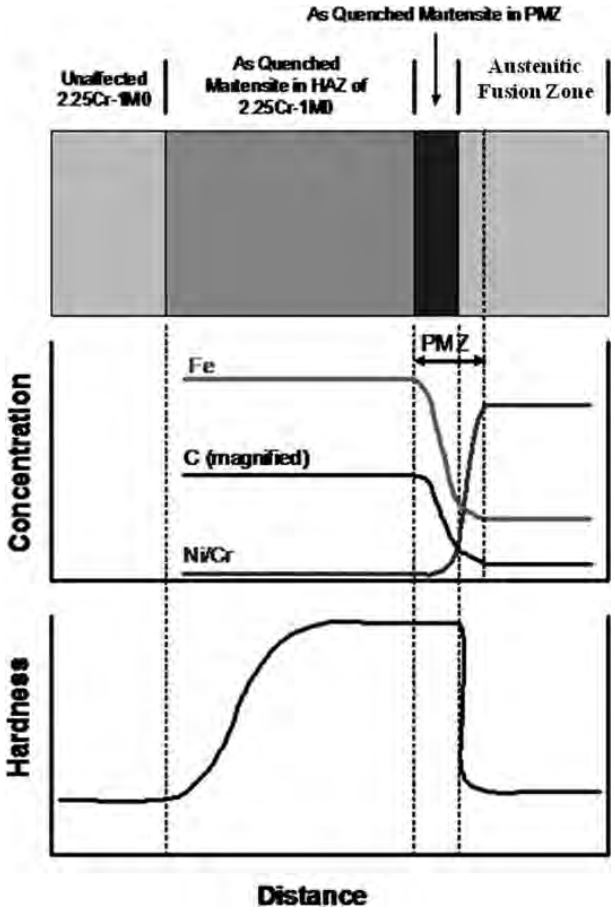

17 Schematic illustration showing general evolution of microstructure in ferritic to austenitic dissimilar welds for as welded condition

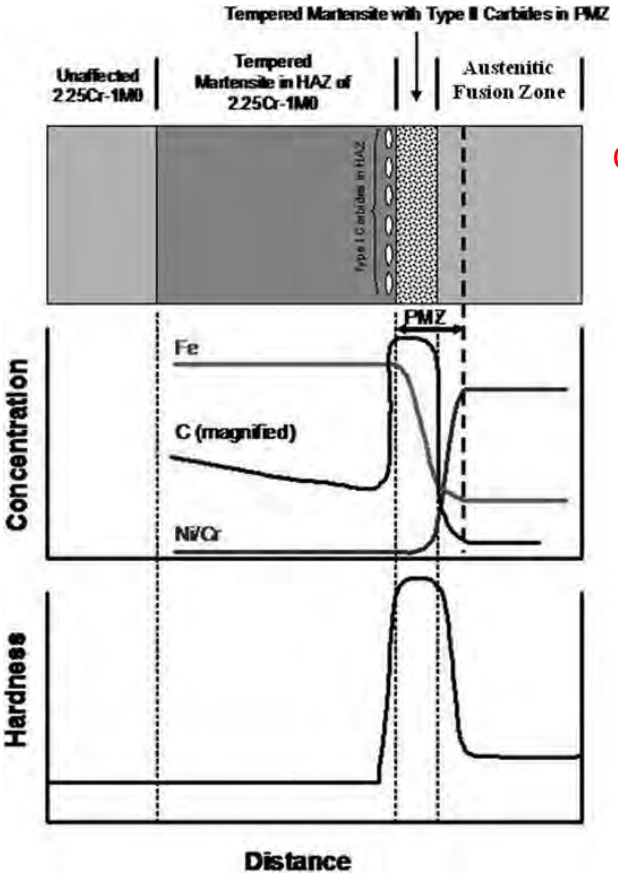

ONLINE COLOUR ONLY

18 Schematic illustration showing general evolution of microstructure in ferritic to austenitic dissimilar welds for aged condition

the as quenched martensite in the PMZ and the austenite region in the fusion zone. As shown in Fig. 18, upon PWHT and/or aging in service, the concentration gradient for the major alloying elements will generally not change significantly, because the diffusion rates of these elements are too low. However, the large change in C concentration, combined with the Cr concentration gradient, produces a C chemical potential gradient that is high in the ferritic steel and low in the austenitic alloy. This leads to C migration from the low alloy steel toward the fusion zone. The PWHT and/or aging will temper the martensite and reduce the high hardness associated with regions that were originally as quenched martensite. However, migration and concomitant enrichment of C leads to the formation of type I and type II carbides in the interface region that produce a highly localised increase in hardness.

Failure mechanism

Numerous investigations have been conducted of both service and laboratory induced failures of DMWs,[5,11–13,15,17,29–34,39–51] and the failure mechanism is now largely understood. There are generally four factors that contribute to premature failure of DMWs during high temperature service:

(i) the difference in CTE between the ferritic and austenitic alloys causes a stress concentration along the interface

(ii) an oxide notch often forms neat the fusion line on the ferritic side of the weld that can concentrate the stress even further

(iii) the highly localised changes in composition and microstructure lead to large differences in creep strength near the interfacial region

(iv) for DMWs prepared with nickel base filler metals, the type I carbides that form along the interface provide a site for nucleation and growth of creep cavities that eventually lead to premature cracking. For DMWs made with stainless steel filler metals, cracking typically occurs along the prior austenite grain boundaries (PAGBs) in the ferritic HAZ at a location of about one or two grains away from the fusion line.

Figure 19 shows examples that highlight various features of DMW failures.[12,32,52] From a macroscopic view, failures occur at the fusion line on the ferritic side of the joint (Fig. 19*a*). An example of oxide notching that can occur on the ferritic side is shown in Fig. 19*b*. The microstructural aspects of the failure are shown in Fig. 19*c* and *d*. Figure 19*c* shows the typical morphology observed for welds made with Ni base filler metals in which failure is initiated along the row of type I carbides that form along the interface. Figure 19*d* shows creep cavitation associated with PAGBs that occurs in welds made with stainless steel filler metals.[12,13] These failure mechanisms are not mutually exclusive. Failures of DMWs made with stainless steel filler metals can often exhibit oxide notches and cracking along both the

International Materials Reviews imr199.3d 28/3/12 16:41:47
The Charlesworth Group, Wakefield +44(0)1924 369598 - Rev 7.51n/W (Jan 20 2003)

ONLINE COLOUR ONLY

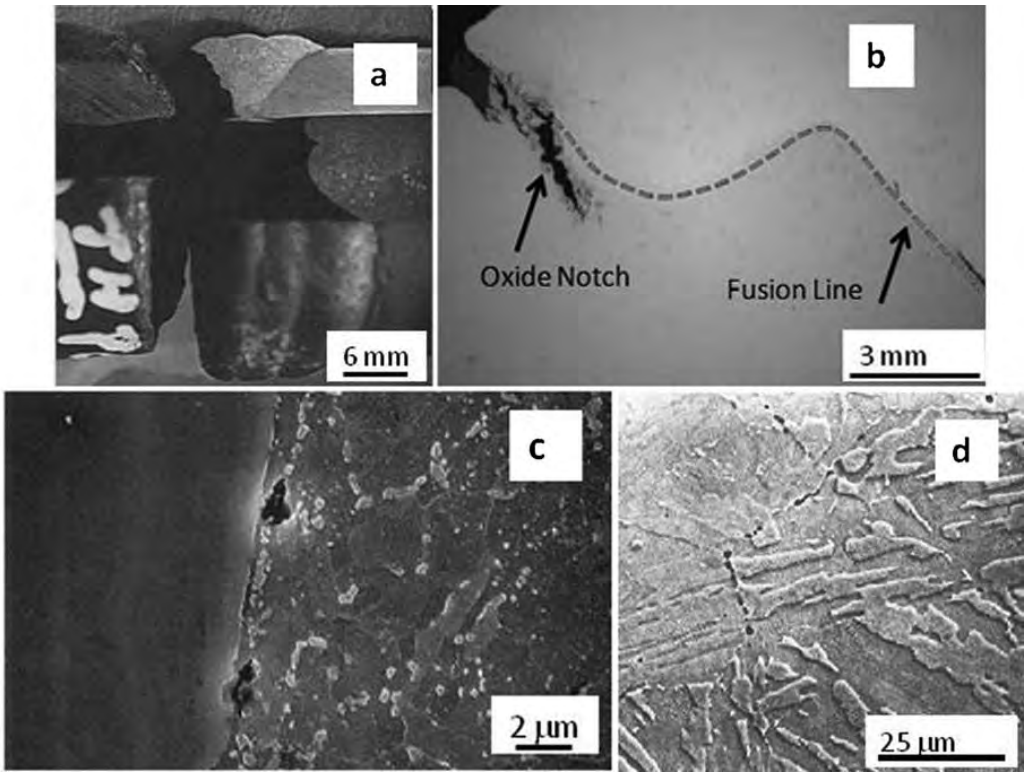

a photograph showing failure along fusion line of ferritic steel; *b* example of oxide notching on ferritic side of weld; *c* creep cavitation along row of type I carbides for welds made with Ni base filler metals;[35] *d* creep cavitation associated with PAGBs in welds made with stainless steel filler metals.

19 Features of dissimilar weld failures: images from *a–c* were acquired from weld made between 2·25Cr–1Mo steel and 316 stainless steel using IN182 filler metal; image from *d* was acquired from weld made between 2·25Cr–1Mo steel and 316 stainless steel using stainless steel filler metal 6

PAGBs and type I carbides. In addition, oxide notching can often be the major contributing factor, particularly in thin walled tubing where the oxide notch can penetrate a significant thickness of the tube and lead to a considerable increase in the local stress.

Figure 20 shows the temperature dependence of the CTE for a variety of materials pertinent to DMWs. Note that rather larger differences in CTE exist between 2·25Cr–1Mo steel and austenitic stainless steels. This large difference in CTE, combined with the large differences in creep strength across the interface, lead to highly localised shear stresses along the fusion line when a stainless steel filler metal is used.[53,54] These stresses can be exacerbated even further due to formation of the oxide notch that can develop in the ferritic side of the weld. The oxide notch has been attributed to the relatively poor oxidation resistance of the 2·25Cr–1Mo steel and localised strain near the fusion zone that can lead to repetitive oxide spallation.[30,39] Thus, thermal cycling can intensify this factor. The differences in CTE mismatch can be reduced by the use of a trimetallic joint involving alloy 800 (UNS N08800) with ERNiCr-3 filler metal.

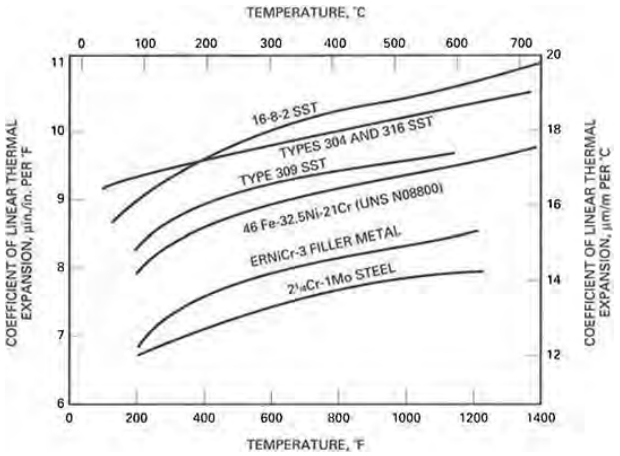

20 Temperature dependence of coefficient of linear expansion for selected base and weld metals used in construction of dissimilar metal weldments

Recent experimental studies[5,31] have confirmed that most of the strain that occurs during creep deformation is associated with the localised strain near the interface. Figure 21 shows results from an instrumented creep test on a weld involving 2·25Cr–1Mo steel and Inconel 82 filler metal where the extension was measured globally (i.e. within the entire gage length) and locally along the interface. The creep tests were conducted at 625°C in air with a stress of 60 MPa. The extension near the interface was recorded at the top and side of the fusion line. Note that Fig. 21 plots the global and local values of the actual extension (not strain), and the amount of global and local extension during creep are very similar. This confirms that most of the deformation is localised near the interface due to the large strength gradients at that location. The influence of environment on the creep behaviour of DMWs is shown in Fig. 22.[32] In these tests, welds involving 2·25Cr–1Mo steel and Inconel 82 filler metal where tested at 625°C and 60 MPa. Two samples

International Materials Reviews imr199.3d 28/3/12 16:42:04
The Charlesworth Group, Wakefield +44(0)1924 369598 - Rev 7.51n/W (Jan 20 2003)

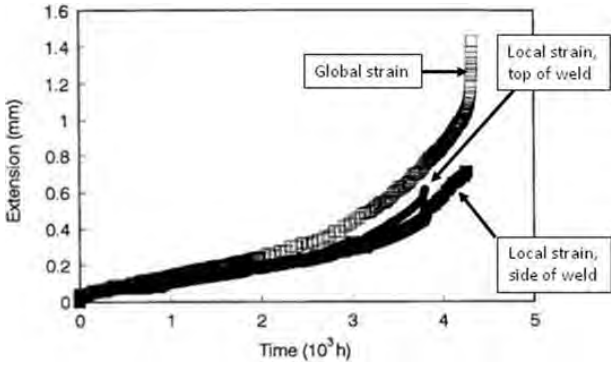

21 Creep rate from instrumented creep test on weld involving 2·25Cr–1Mo steel and Inconel 82 filler metal where extension was measured globally (i.e. within entire gage length) and locally along interface at top and bottom of weld: creep tests were conducted at 625°C in air with stress of 60 MPa

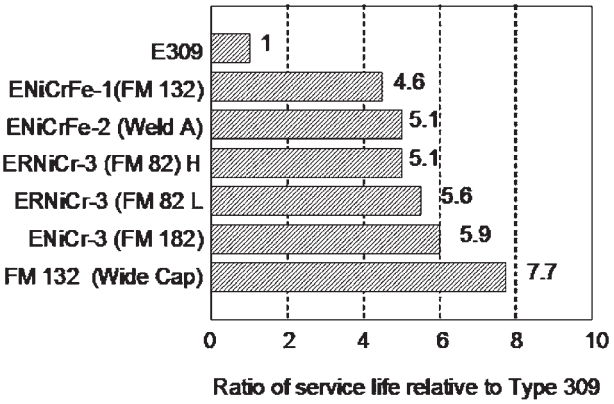

23 Comparison of relative creep life of welds from industrial survey showing effect of filler metal on service life of dissimilar welds (relative to 309 filler metal)

were initially tested in air, while one sample was coated (coating type not specified) to protect the surface from oxidation. Note the large differences in creep rate between the coated and exposed samples. After 356 h of exposure, one of the originally uncoated samples was coated and reintroduced into the creep test. This led to a reduction of the creep rate. These results are significant in two aspects. First, they demonstrate that creep testing for purposes of acquiring design data need to be conducted in an environment that closely simulates that expected in service. Second, the results indicate that considerable improvements in creep resistance should be possible with the application of protective coatings. Unfortunately, this area has not received considerable attention.

It is important to note that there are various sources of stress beyond those due to normal operation that contribute to premature failures and need to be considered from a design perspective.[13,33] The stress sources are typically divided into one of four categories:

(i) operating stresses that arise from pipe weight, internal pressure, and thermal gradients through the wall thickness
(ii) stresses that result from CTE mismatch and residual stresses from welding
(iii) system stresses that arise due to mechanical constraints of thermal expansion
(iv) cyclic stresses due to thermal cycling that are induced due to CTE and strength mismatch

Most of the early premature failures of DMWs involved those in which ferritic steel was joined to stainless steel using a stainless steel filler metal. It was initially suspected that failure occurred within the decarburised region due to the relatively poor creep strength at that location. However, more detailed examinations acquired from service failures[13,33] have demonstrated that failure is initiated along PAGBs in the ferritic steel HAZ (for welds made with stainless steel filler metals). Thus, although the presence of the C denuded zone may exacerbate the problem by producing steep gradients in strength mismatch along the interface, it does not appear to be a necessary condition for failure. The welding of ferritic to stainless steels is now typically performed with transition joints and Ni base filler metals. The most commonly used transition joint utilises an alloy 800H section that is inserted between the ferritic and stainless steel alloys, and an ERNiCr-3 filler metal is used. This joint design minimises CTE mismatch along the interface.

As shown in Fig. 23, an industrial survey[55] has shown that the use of the transition joint design typically extends the service life of DMWs by a factor of ~5 compared to direct welds between ferritic and stainless steels made with stainless steel filler metals. A wide cap on the 2·25Cr–1Mo steel (in which the bevel angle of the joint is increased near the surface of the weld) has also been

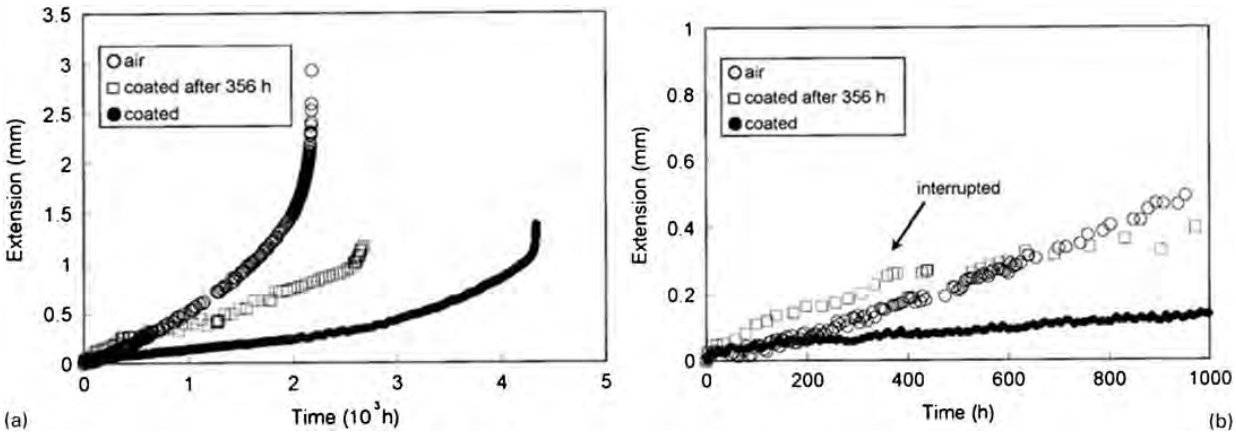

a strain rate out to ~4500 h; *b* results for early stages of creep out to 1000 h

22 Creep rates for weld involving 2·25Cr–1Mo steel and Inconel 82 filler metal showing influence of environment on creep behaviour: creep tests were conducted at 625°C in air with stress of 60 MPa

International Materials Reviews imr199.3d 28/3/12 16:42:16
The Charlesworth Group, Wakefield +44(0)1924 369598 - Rev 7.51n/W (Jan 20 2003)

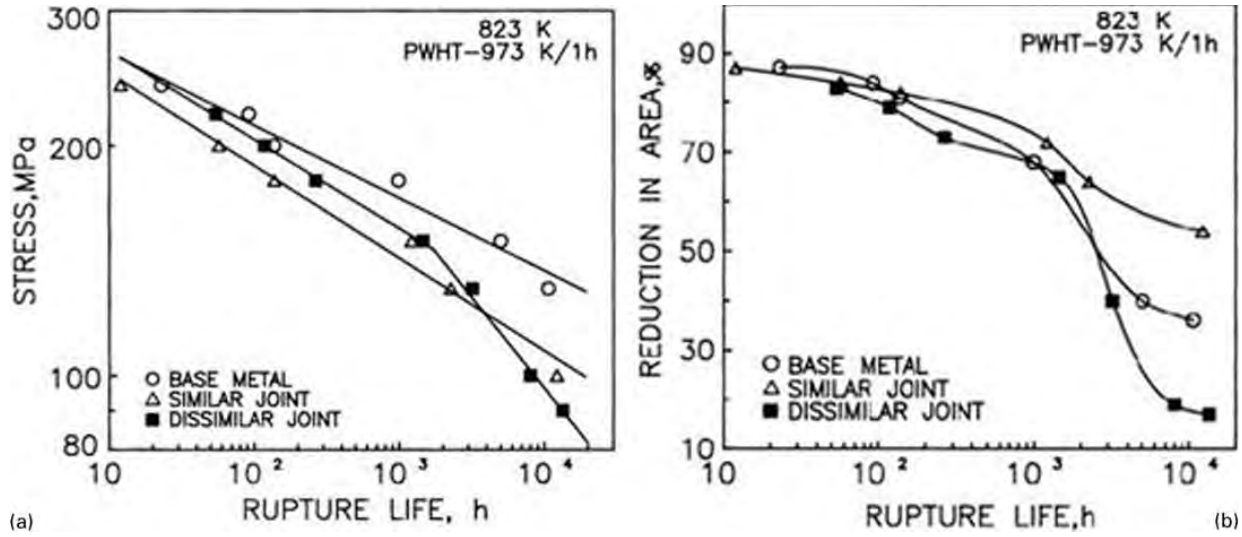

24 ***a*** **creep life and** ***b*** **ductility of welds between 2·25Cr–1Mo steel and alloy 800H at 550°C over stresses from 90 to 250 MPa: data are shown for 2·25Cr–1Mo base metal, 2·25Cr1Mo-to-2·25Cr1Mo similar joint, and a dissimilar joint between 2·25Cr–1Mo and alloy 800H.**

shown to provide further improvement, presumably due to a reduction in stress concentration along the interface. The wide cap is accomplished by simply increasing the bevel angle of the joint near the surface of the weld.

Creep rupture properties

Many investigators have attempted to develop creep rupture data of DMWs, in order to determine the effective service life for a given set of stress, temperature and environmental conditions. A review of the data developed to date indicates this can be a difficult task due to the complex changes in microstructure that evolve during aging. Creep tests conducted at stresses significantly higher than those expected in service often produce short failure times in which the microstructure partially responsible for failure does not have enough time to properly develop. As a result, the failure mechanism observed in the field is not properly replicated in the laboratory and the usefulness of the data is therefore questionable. Similarly, the environment can play an important role in reducing the overall life due to preferential oxidation.[31,32] This effect can, in turn, be influenced by the test sample diameter when the size of the degraded zone becomes an appreciable fraction of the sample diameter. This raises the applied stress on the sample significantly beyond the nominal applied stress associated with the test. Creep tests conducted under parameters that more closely simulate the actual service conditions obviously provide data that are more accurate for life time predictions, but these tests may be prohibitively long and expensive. In view of these factors, creep testing of DMWs requires careful consideration, in order to utilise tests that provide meaningful data within reasonable test times. The data available are reviewed in this section for the purposes of:

(i) comparing available creep rupture data of DMWs to that of existing data on 2·25Cr–1Mo base metal and welds that are used for design purposes
(ii) identifying important factors that need to be considered in future testing
(iii) identifying methods that may provide improved performance.

Laha *et al.*[5] recently investigated the creep strength of welds between 2·25Cr–1Mo steel and alloy 800H made with IN182 filler metal at 550°C over a range of stress from 90 to 250 MPa. Comparison was made between 2·25Cr–1Mo similar welds and base metal. The welds were given a typical PWHT of 700°C for 1 h before testing. Results of the rupture life and reduction in area are shown in Fig. 24. Similar welds of 2·25Cr–1Mo steel typically exhibit reduced failure times compared to the base metal. This has been attributed to the inferior creep resistance of recrystalised grains in the intercritical portion of the HAZ. The dissolution of Mo_2C carbides within this region during the weld thermal cycle has also been cited as a contributing factor to early fracture.[56–59] The DMW appears to provide better creep life than the similar weld at high stresses and short rupture times. However, at stresses below ~130 MPa, the life of the DMW is below that of the similar 2·25Cr–1Mo weld. A difference in failure mode of the DMW was also observed with changes in applied stress level. At stresses above 150 MPa, extensive necking of the ferritic steel was observed and failure occurred in the intercritical region of the 2·25Cr–1Mo steel HAZ. As shown in Fig. 24*b*, this produced failures with rather high ductility. At stresses below 150 MPa, failure occurred by intergranular creep cavitation in the coarse PAGBs of the 2·25Cr–1Mo steel with relatively little ductility. The low ductility occurs because most of the deformation is localised along the weld interface, which is typically observed in field failures.

Fracture along the coarse PAGBs that occurred at the lower stress levels is similar to that which occurs in relatively short times in the field for welds made with stainless steel filler metals.[12,13,17] However, the observed failure modes associated with the data in Fig. 24 at both low and high stresses do not properly simulate that observed in service for welds made with Ni base filler metals. (i.e. creep cavitation at type I carbides). The authors noted that some creep cavities started to develop around the interfacial carbides, but these were not

International Materials Reviews imr199.3d 28/3/12 16:42:23
The Charlesworth Group, Wakefield +44(0)1924 369598 - Rev 7.51n/W (Jan 20 2003)

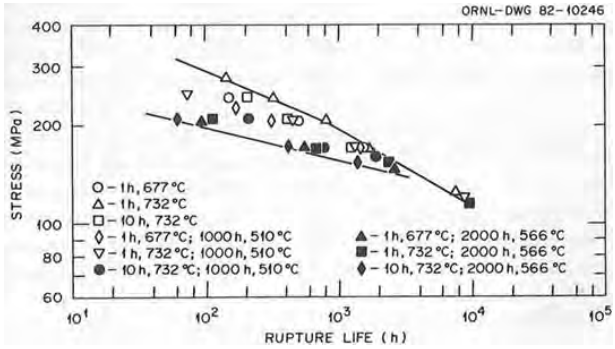

25 Influence of PWHT condition and aging treatments on creep properties of 2·25Cr–1Mo steel/alloy 800H joints at 510°C (prepared with ERNiCr-3 filler metal)

associated with the final fracture. This indicates that the stresses were too high, and the corresponding test times too low to permit development of the interfacial microstructure and stress state responsible for failures observed in the field.

Klueh and King[39] conducted tests on the same DMW combination. The influence of various PWHT conditions and aging treatments on the creep properties of the joints at 510°C were evaluated. A summary of their test results is shown in Fig. 25. Note that most of the applied stresses are well above 100 MPa. All but three samples exhibited high ductility failures (>65% reduction in area) that occurred in the 2·25Cr–1Mo steel, which are not typical of those observed in service. The effect of aging, either in the form of PWHT or artificial aging, is to reduce the rupture life. This occurs because the aging reduces the creep strength of the 2·25Cr–1Mo steel (where the failure occurs). The three samples that failed at longer times exhibited fractures near the fusion line in a fashion similar to that described above by Laha *et al.*[5] Klueh and King suggested that the failure of DMWs under both test and plant conditions is dominated by oxide notch formation that is driven by a chromium depleted region in the 2·25Cr–1Mo steel near the interface. As discussed above, the oxide notch can be an important factor in many DMWs, but it is not the primary cause of failure.

Parker and Stratford[31,32] recently recognised the importance of test conditions for accurately simulating the failure mode observed in the field. They conducted tests at temperatures of 590, 605 and 625°C and reduced stresses of 30–80 MPa. The reduced stresses were used in an attempt to provide increased failure lives and therefore more closely simulate the field failure mode. The influence of aging was also considered. Samples were tested in the 'new' condition, which only received a typical PWHT of 700°C for 3 h. 'Aged' samples were given the identical PWHT treatment in addition to a thermal treatment of 625°C for 3500 h. This treatment was performed in order to nucleate and grow the type I interfacial carbides that are known to induce form creep cavities that eventually lead to failure. Their data are provided in Fig. 26. The new weld samples exhibited failure at the interface with very low ductility via creep cavitation along the type I carbides for all stress and temperature combinations considered. The aged samples exhibited ductile failure (typically >90% reduction in area) in the 2·25Cr–1Mo steel away from the weld area at stresses of 60 MPa and above. At applied stresses of 50 MPa and below, failure of the aged welds occurred by creep cavitation around the type I carbides. Thus, the conditions of this test (<50 MPa) most accurately simulate service failures. Most of the failure times associated with these tests were between 1000 and 10 000 h, which are considerably longer than those used previously in higher stress tests.

The difference in stress levels needed to simulate field failures (stress $\leqslant$50 MPa in the aged welds, stress $\leqslant$80 MPa in the new welds) can be attributed to the tempering effect that the aging treatment had on the 2·25Cr–1Mo steel. Aging at 625°C for 3500 h decreases the creep strength of the ferritic steel. Thus, the higher stress levels produce considerable creep deformation in the aged ferritic steel to the point where failure occurs by plastic instability associated with necking. This effect probably accounts for the relatively short failures times at 80 MPa for the aged samples (and concomitant reduced slopes of the stress versus temperature plots for the aged samples in Fig. 26.) In the new samples, the creep strength of the 2·25Cr–1Mo steel is higher so that deformation is more localised along the interfacial region and leads to failure along this region. It is important to note that, although actual service temperatures may be below the 590–625°C range considered in this work, the actual service lifetimes will be well beyond the aging and failure times of 3500 to ~10 000 h respectively. Thus, considerable softening of the 2·25Cr–1Mo steel in service is expected, and applied stress levels below ~50 MPa should be included in future creep tests

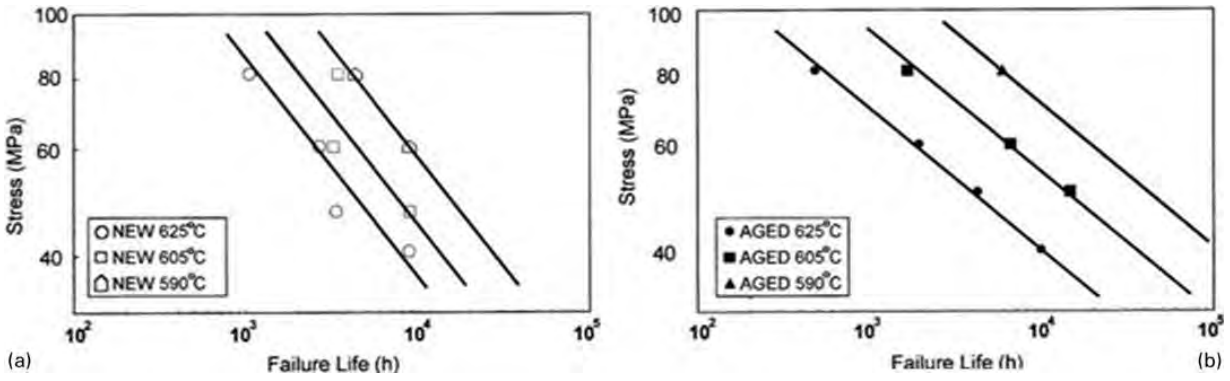

a 'new' condition; *b* 'aged' condition

26 Results from creep tests at temperatures of 590, 605 and 625°C for welds between 2·25Cr–1Mo steel and 316 stainless steel made with Inconel 82/182 filler metal

International Materials Reviews imr199.3d 28/3/12 16:42:30
The Charlesworth Group, Wakefield +44(0)1924 369598 - Rev 7.51n/W (Jan 20 2003)

ONLINE COLOUR ONLY

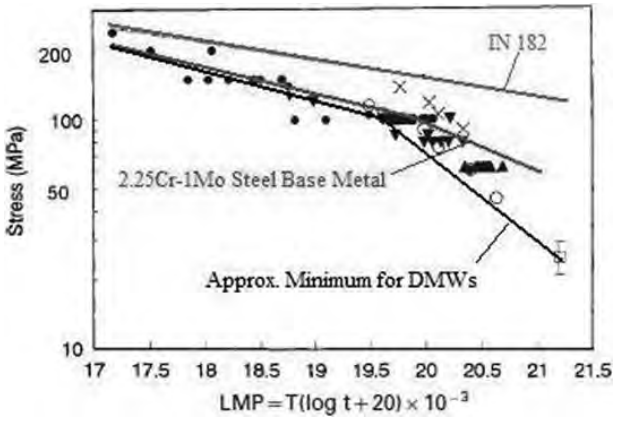

27 Larson–Miller plot of creep rupture data for wide range of dissimilar welds involving ferritic steel and Inconel type filler metals

in order to simulate service type failures. This aspect requires careful consideration in future test programs.

There was relatively little difference in failure lives between the new and aged samples that fractured via creep cavitation. It might be expected that excessive PWHTs and/or thermal aging will accelerate formation of type I carbides and therefore lead to premature failure times. The similarity in rupture lives between the new and aged welds indicates that pre-existing carbides do not accelerate creep cavitation. This implies that a critical amount of strain is required for creep cavitation to occur, and PWHT is not necessarily detrimental. The deleterious effects of PWHT cited to date[39] from laboratory tests can actually now be understood. Most of these data were generated for higher stress levels where failure occurred in the 2·25Cr–1Mo steel due to a reduction in creep strength, but this failure mode is not typical of that observed in service. Thus, when tests are conducted under conditions that properly simulate the DMW failure mode, PWHT does not appear to have a deleterious influence on service life.

Figure 27 shows creep rupture data in the form of a Larson–Miller plot for DMWs from a wide range of sources.[13] Many of the welds were made using Inconel type filler metal that is similar to that currently used for joining low alloy steels to stainless steels. The low stress/long time data are particularly useful since these samples generally simulated the interfacial failure mechanism observed in the field. The creep behaviour for 2·25Cr–1Mo steel and Inconel 182 filler metal are shown (as solid lines) in Fig. 27 for comparison. Note that, for the limited data available, the reduction in failure life for the DMWs compared to the 2·25Cr–1Mo steel base metal appears to increase as the stress level is reduced. Additional creep data are needed to more clearly establish the long term performance of DMWs relative to the ferritic base metal.

It is useful to consider additional factors beyond stress and temperature that may influence the creep rupture life of DMWs. This information could be useful for future test programs in order to improve the consistency of results between various laboratories and also establish the relative influence of secondary factors on creep life. This latter point could also be useful for improving the performance of DMWs in service. Some of the important secondary factors that affect the creep life include the test environment (e.g. air versus inert atmosphere), sample size, groove angle of the weld and filler metal composition. The test environment can clearly have a large influence on the creep rupture time through formation of an oxide notch, and the effect can be particularly strong at high temperatures and small sample sizes. High temperatures can induce an artificially high effect from the oxide notch, because the oxidation rate increases rapidly with increasing temperature. In addition, the oxide will form a larger stress concentration and produce an overall increase in the applied stress as the sample size is reduced. This influence is observed in field failures, where oxide notching can play a significant role in failures of thin walled tubes, but becomes less important for heavy wall pipes. This points to the need to develop coatings that could be used to eliminate the oxide notch effect, which would provide two advantages. First, it could lead to improvements in creep life, particularly for thin walled tubing. Second, it would permit test results conducted in inert environments (or on coated samples) to provide a more accurate representation of the performance expected in service.

The influence of weld groove angle on creep life appears to warrant further consideration. The results of finite element (FE) modelling by King *et al.*[53] suggest that the peak stresses in the weld can be reduced with a reduction in the weld groove angle. However, industrial experience suggests that wider groove angles improve service life. It is interesting to note that review of a large database for similar welds in 2·25Cr–1Mo steels[50] also did not reveal any systematic influence of weld groove angle. Future work that combines FE modelling with experimental verification appears necessary to resolve this issue. The influence of filler metal type is now established and has already been discussed, where Ni base filler metals provide a significant increase in life over stainless steel filler metals due to reduced C migration and improved CTE matching.

Aging behaviour of filler metal

The fusion zone of welds made with ERNiCr-3 filler metal will also undergo microstructural changes during high temperature aging that have been shown to affect the low temperature mechanical properties of the weld. This has been investigated by Klueh and King[61,62] and more recently Sireesha *et al.*[15,63] Klueh and King[61] aged ERNiCr-3 weld metal at temperatures between 510 and 677°C for up to 15 000 h. The influence of aging time and temperature on the yield strength and ductility are shown in Fig. 28, where a significant increase in strength and reduction in ductility is observed during aging. Sireesha *et al.*[15,63] observed a similar effect on the toughness of welds made between 9Cr–1Mo steel and alloy 800H using ERNiCr-3 filler metal that were aged at 625°C for up to 5000 h. The changes in hardness and impact toughness of the welds are shown in Fig. 29, where an increase in hardness and reduction in impact toughness are readily apparent. The notches for the charpy impact tests were placed in the fusion zone where the weld metal resides. Thus, the results can be compared with the all-weld metal data in Fig. 28.

These increase in strength and reduction in ductility and toughness described above have been attributed to both short range ordering and precipitation that occurs in the temperature range of ~500 and 680°C. Klueh and

International Materials Reviews imr199.3d 28/3/12 16:42:38
The Charlesworth Group, Wakefield +44(0)1924 369598 - Rev 7.51n/W (Jan 20 2003)

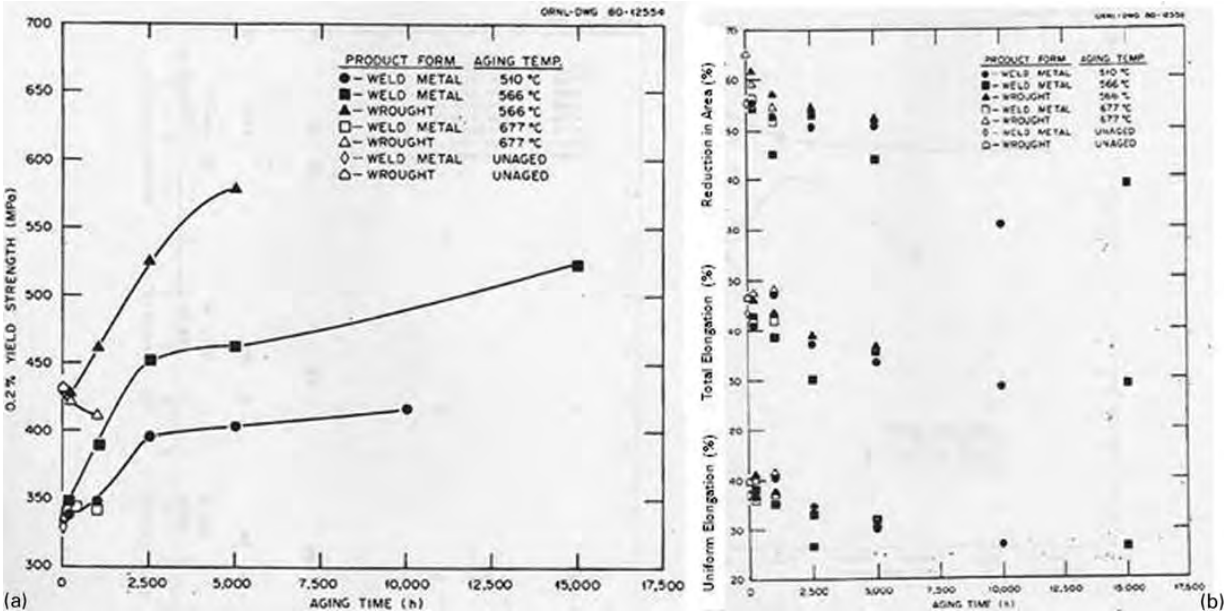

a 0·2% offset yield strength as function of aging time; *b* ductility (in terms of uniform elongation, total elongation and reduction in area) as function of aging time

28 Tensile tests data for dissimilar welds involving ferritic steel and Inconel type filler metals: tests were conducted at room temperature at strain rate of 3×10^{-6} s^{-1}

King[61] observed precipitation within the weld and identified both precipitation and short range ordering to be responsible for the property changes, but did not identify the precipitates involved. Siressha *et al.*[15] identified the precipitates as $M_{23}C_6$, Ni_3Ti and NbC. Images (SEM) of the charpy impact test specimens in the as welded and aged conditions are shown in Fig. 30. The as welded sample exhibits typical microvoid coalescence and a relatively fine dimple spacing. The aged sample also exhibits evidence of microvoid coalescence along with evidence of precipitates on the fracture surface. The precipitates and long range order are expected to contribute to increased strength and decreased ductility. The precipitates can also lead to premature fracture by accelerating the microvoid coalescence process, since they provide sites for decohesion between the particles and matrix. Although the ductility and toughness are still relatively high (i.e. total elongation values are above 30% and impact toughness values are >50 J), the changes are nonetheless significant and should be noted.

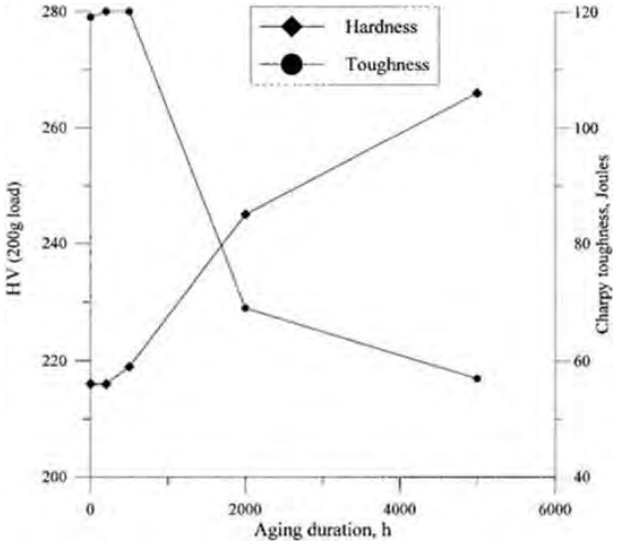

29 Variation in room temperature hardness and impact toughness of fusion zone for welds between 9Cr–1Mo steel and alloy 800H (made using ERNiCr-3 filler) that were aged at 625°C

Remaining life estimation techniques

The potential for premature failure of DMWs provides impetus for development of techniques for estimating the remaining life of components in service. Several approaches to this problem have been proposed and are worth noting. In the simplest sense, the condition of DMWs can be qualitatively assessed using metallographic techniques to examine the condition of the weld. Since the microstructural mechanism of failure is known (i.e. creep cavitation at type I carbides followed by micro- and macrocrack formation), direct examination of metallographic samples and/or replication techniques can be applied to evaluate the extent of damage. The qualitative relation between damage morphology and remaining life for homogenous wrought materials is known and shown schematically in Fig. 31, where the microvoid and crack morphology is qualitatively related to remaining life.[64] This qualitative relation requires modification to account for the unique fracture features of DMWs. With this approach, the inspection frequency is typically increased when isolated creep cavities are first identified, and component replacement would occur before the link up of creep cavities. The challenge to this approach is proper identification of critical components, and locations within each component, that are most vulnerable to creep damage. This can be difficult when one considers that the area utilised for examination is an extremely small fraction of the potential volume of material that may be subjected to damage. Results from FE thermal and stress modelling should be combined with plant history data, in order to guide such an assessment, and all the various sources of stress

International Materials Reviews imr199.3d 28/3/12 16:42:40
The Charlesworth Group, Wakefield +44(0)1924 369598 - Rev 7.51n/W (Jan 20 2003)

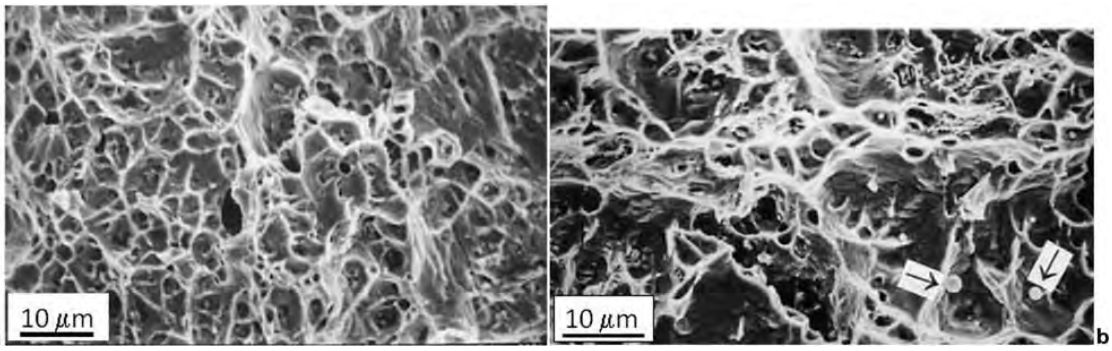

30 images (SEM) of Charpy impact specimens (tested at room temperature) in *a* as welded condition and *b* aged for 5000 h at 625°C

previously described should be considered. An additional concern with the replication technique is that failure may not always be most severe on the component surface where the replication is acquired. In fact, some service inspections[33,65] indicate that void formation and cracking can initiate within the interior of the wall.

Figure 32 shows recent laboratory data that may serve as the basis for potentially providing a more quantitative approach to the relation between cavitation and remaining life fraction.[31,32] These data show the maximum amount of cavities (measured in number of cavities per unit length along the interface) as a function of life fraction for DMWs between 2·25Cr–1Mo steel and 316 stainless steel welded with Inconel 82 and 182 filler metals. The butt welds were made on pipes with a 368 mm outside diameter and wall thickness of 35 mm. Data for all the 'new' welds and for 'aged' welds that exhibited low ductility failure, generally lie on a single curve. These samples all fractured by creep cavitation at type I carbides. The aged samples tested at higher stresses failed in the 2·25Cr–1Mo steel and thus do not replicate field conditions. Note that data for these welds generally fall outside of the curve. It was noted that a cavity density of about 400 cavities/mm existed just before crack formation, and this corresponded to ~85% of the creep life. The instantaneous cavity density N at any given life fraction t can then be related to the cavity density at fracture N_f associated with the end of life t_f. The authors propose a relationship of the form

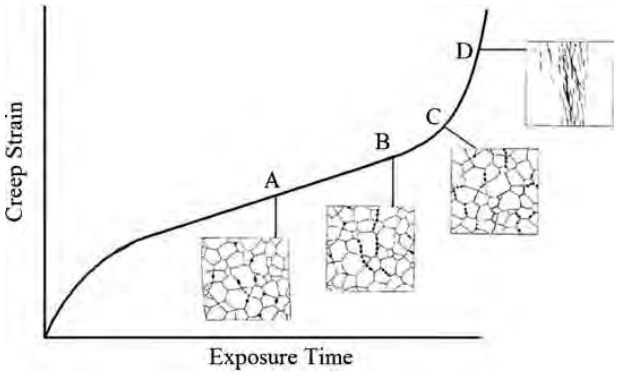

31 Schematic creep curve in tension showing appearance internal voids which develop *a* during steady state creep, *b* at onset of tertiary creep, *c* in tertiary creep and *d* at failure

$$\frac{t}{t_f} = 1 - \left(1 - \frac{N}{N_f}\right)^{\lambda} \tag{3}$$

where λ is the Monkman–Grant constant. Figure 32*b* shows experimental data along with a plot of equation (3) using a value of $\lambda = 2{\cdot}5$, and a reasonable correlation is obtained. Additional data are needed, particularly from well documented field studies, to provide further experimental verification of this potential technique. It should also be noted that this approach is subject to the same challenges described above for metallographic and/or replication techniques.

A method has also been proposed for direct calculation of the damage fraction from operating parameters.[33,65] The technique, known as prediction of damage in service (PODIS), considers total damage D_{TOT}, to develop from three sources

$$D_{TOT} = D_I + D_P + D_S \tag{4}$$

where D_I is the intrinsic damage associated with temperature cycling due to changes in power loads, D_P is damage associated with primary loads during steady state operation that include both pressure and component weight and D_S is damage from secondary bending loads that arise from load cycling and creep rupture that accumulates during hold periods. Loads associated with the latter factor are considered strain controlled. They will relax at elevated temperature, but will be regenerated during temperature cycling. The value of D_{TOT} is specifically defined as the amount of interfacial area that has suffered damage due to voiding/cracking and is therefore not capable of sustaining a load. For example, if A_o is the original interfacial area of the weld before service and A_i is the amount of remaining interfacial area that has not been damaged after some service time (and therefore capable of carrying the load), then D_{TOT} is given by

$$D_{TOT} = \frac{A_o - A_i}{A_o} \tag{5}$$

The technique is divided into two failure scenarios. Mode I failure is associated with intergranular cracking along PAGBs within the HAZ of the ferritic steel. As described above, this occurs in welds made with stainless steel filler metals. Mode II failure involves creep cavitation and cracking along type I carbides associated with welds made using Ni base filler metals. For mode II failure, D_I is considered negligible due to the small difference in CTE 7

International Materials Reviews imr199.3d 28/3/12 16:42:50
The Charlesworth Group, Wakefield +44(0)1924 369598 - Rev 7.51n/W (Jan 20 2003)

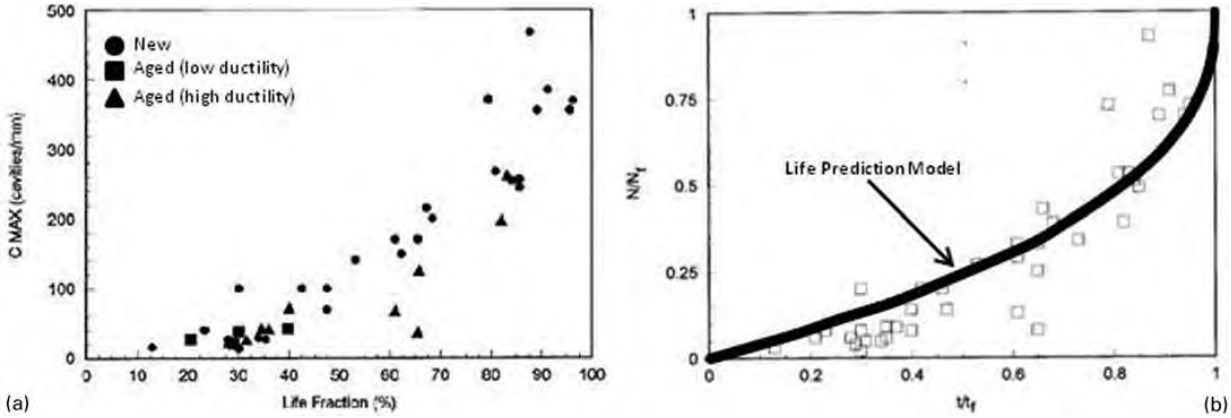

32 ***a*** **maximum amount of cavities (measured in number of cavities per unit length along interface) as function of life fraction for DMWs between 2·25Cr–1Mo steel and 316 stainless steel welded with Inconel 82 and 182 filler metals and** ***b*** **experimental data along with plot of equation (3) using value of** $\lambda=2{\cdot}5$

between the weld metal and ferritic steel. The values of D_P and D_S for this case are then given by

$$D_P = \sum_{1}^{m} k_1 t_m 10^{f(T_o)} \left[\frac{\sigma_P}{1-k_2 10^{g(T_o)} t_n^{1/3}}\right]^{\beta} \quad (6a)$$

$$D_S = \sum_{1}^{m} k_3 n(\varepsilon_S)^{\gamma} + k_4 t_m 10^{f(T_o)} \left[\frac{\sigma_S}{1-k_5 10^{g(T_o)} t_n^{1/3}}\right]^{\beta} \quad (6b)$$

where m is number of loading conditions, σ_P is primary axial stress, σ_S is secondary axial stress, t_m is incremental time for a constant σ_P, t_n is cumulative time from $t=0$ up to t_m, T_o is average operating temperature at steady state loading conditions m, $f(T_o)$ and $g(T_O)$ are functions of T_o, ε_S is strain range and k^1, γ, β are constants.

Ryder and Dahms[65] provide more details on values of the constants and the calculation procedure. The values for the required constants were determined from both laboratory and field data. Predictions were then compared with additional data obtained from controlled laboratory experiments or well documented samples removed from actual plants. This approach assumes that failure occurs by creep void formation along the row of interfacial carbides, which has been verified experimentally. It also assumes the intrinsic damage in welds made with Ni base alloys is negligible and that the damage estimate can be obtained by linearly summing the damage from the remaining two components (D_P and D_S). The first assumption is apparently invoked due to the reduced CTE mismatch associated with the use of nickel base filler metals.

Figure 33 shows a comparison of the calculated damage to that observed experimentally, where the dotted lines are for a 95% confidence interval. Reasonable agreement is obtained between the measured and calculated values. There are, however, a number of instances where the predictions are non-conservative. It is possible that additional data may be helpful for refining the constants and improving the accuracy of the predictions.

Best practices

The practices that are currently utilised to maximise the life of DMWs have been described in the various sections above. They are briefly summarised here, due to their importance during construction and operation. The major fabrication variables that must be considered include joint design, filler metal type and application of PWHT. Operational variables of major importance include operating temperature, temperature cycling, stress, and environment. The optimal design that is currently used for joining ferritic steels to stainless steels is one that consists of a low alloy steel/alloy 800H/stainless steel trimetallic joint. Inconel 82 and/or 182 filler metals are used for each of the two joints involved with this trimetallic member. These transition sections are typically fabricated in the shop and then two similar welds are made in the field. This trimetallic transition approach helps reduce interfacial stresses associated with CTE mismatch. The improvement in service life associated with the use of Ni base filler metals has been verified by both laboratory testing[66] and industry surveys.[55]

Early results[39] suggested that application of a PWHT was detrimental to the inherent creep life, particularly when conducted at elevated temperatures and long times. This may apply to welds involving stainless steels where C migration and CTE mismatch is rather extensive. Early concerns on the use of a PWHT may have arisen due to the potential to nucleate and grow the carbides along the fusion line that are known to contribute to premature

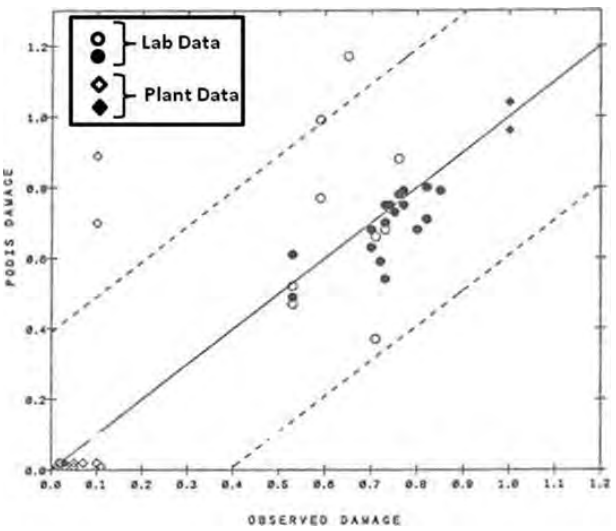

33 Comparison of calculated damage to that observed experimentally using PODIS method, where dotted lines are for 95% confidence interval

International Materials Reviews imr199.3d 28/3/12 16:42:56
The Charlesworth Group, Wakefield +44(0)1924 369598 - Rev 7.51n/W (Jan 20 2003)

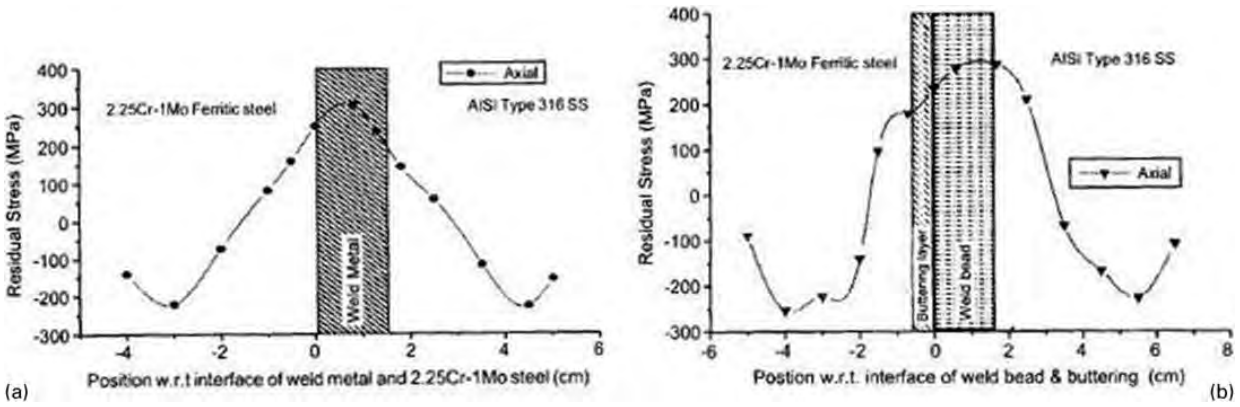

a as welded condition; *b* weld prepared with 6 mm 'butter' layer of Inconel 82 on 2·25Cr–1Mo steel, exposed to PWHT at 725°C for 1 h, and then welded to 316 stainless steel using same filler metal (measurements were made on ~20 μm of top surface layer of weld after measurement locations were electrolytically polished)

34 Residual axial stress distribution of welds between 2·25Cr–1Mo steel and 316 stainless made with Inconel 82 filler metal

creep failure. However, more recent results of well controlled laboratory studies have shown that use of a PWHT does not alter the inherent creep life in any significant way.[31,32,35,67] Nicholson examined the influence of PWHT at 700°C on the carbide size and distribution for times up to 8 h.[35,67] He observed that application of a PWHT had a relatively minor effect on the carbides compared to subsequent aging in service. This is supported by available creep data that demonstrate the creep life of DMWs is similar in the as welded and PWHT conditions.[31,32,68] Use of a PWHT is therefore expected to provide an overall beneficial effect due to relief of residual stress. Verification of this has recently been provided through residual stress measurements.

Joseph *et al.*[69] recently measured the residual stresses in DMWs made in the as welded and PWHT condition. Welds were fabricated between 2·25Cr–1Mo steel and 316 stainless steel using Inconel 82 filler metal with the gas tungsten arc welding process. The pipe was 19·4 cm in diameter with a 8 mm wall thickness. One weld was first prepared with a 6 mm 'butter' layer of Inconel 82 on the 2·25Cr–1Mo steel, exposed to a PWHT at 725°C for 1 h, and then welded to the 316 stainless steel using the same filler metal. This buttering technique is used to avoid PWHT of the 316 stainless steel that may sensitise that alloy. The residual stress was also measured on a weld made directly between 2·25Cr–1Mo steel and 316 stainless steel (using the same filler metal) without a PWHT. Figure 34 compares the axial residual stresses from each weld. The axial stresses are shown because they are the most important orientation from a creep damage point of view. The hoop stresses were also measured and showed similar trends. As shown in Fig. 34*a*, a maximum tensile axial stress of 350 MPa is observed in the center of the weld metal in the as welded condition. The interface between the weld metal and 2·25Cr–1Mo steel is the most important location, since this is where failure is known to occur. The residual axial stress at this location is 260 MPa in the as welded condition. As shown in Fig. 34*b*, these values are reduced considerably for the weld exposed to a PWHT, where the maximum stress at the weld centerline is reduced to 300 MPa, and the interfacial stress is reduced to 180 MPa. Use of longer times may provide additional stress relief and warrants further examination. Thus, considering that PWHT provides significant stress relief and no observable reduction in creep rupture life, use of this heat treatment should be beneficial for extending the life of DMWs. Results from industrial surveys also suggest that large included angles and additional weld reinforcement are beneficial for increasing service life.[55] As mentioned above, additional experimental results and FE analysis would be useful for understanding the influence of these factors in more detail.

The microstructural changes and preferential oxidation that occur during aging are generally thermally activated processes and are therefore expected to increase significantly with increasing temperature. Similarly, higher temperatures and/or large changes in temperature will exacerbate the stresses generated from CTE mismatch. Thus, DMW life is obviously expected to increase with decreasing operating temperature. This is important from a design perspective as it points to the need to place DMWs in regions where the temperature is as low as feasibly possible. Similar comments can be made with regard to stress, and the various sources of stress need to be minimised beyond those associated with normal operation. Abrupt changes in wall thickness between the ferritic and austenitic alloys should also be avoided in order to minimise stress concentrations associated with changes in geometry. Results from industry surveys[55,70] have demonstrated that DMWs are significantly more prone to failure when located in high temperature/high stress conditions, and this points to the need for minimising failures through design strategies that reduce stress and temperature to the fullest extent possible. Lastly, any steps that can be applied to minimise corrosion of the ferritic steel near the interface are expected to extend the service life. This would include placing the DMW in locations of reduced temperature and/or less aggressive environments where excessive oxidation will not occur. It appears that protective coatings, which could possibly be locally applied to the joint interface during fabrication, could offer a means for improved performance.

Research in progress

Work is currently in progress to improve the high temperature performance of welds made between ferritic and austenitic alloys. One study is being conducted to

International Materials Reviews imr199.3d 28/3/12 16:43:04
The Charlesworth Group, Wakefield +44(0)1924 369598 - Rev 7.51n/W (Jan 20 2003)

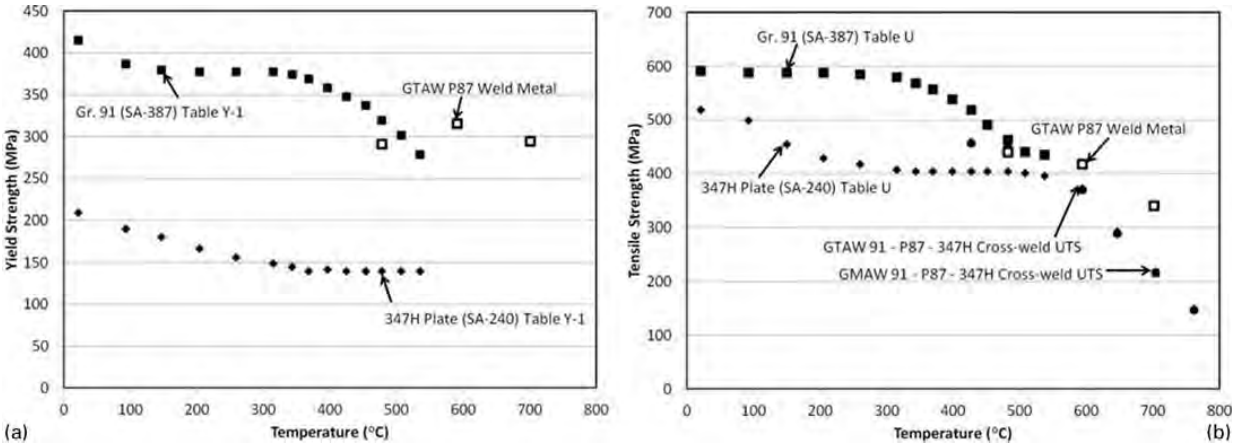

a yield strength; *b* tensile strength

35 Short term/high temperature strength data of all-weld metal and cross-weld samples for dissimilar welds between grade 91 and 347H made with P87 filler metal

develop a nickel base filler metal that can provide an improved CTE match with the ferritic steel and reduce C migration across the fusion line.[24,25] The filler metal is primarily being developed for welds made between 9Cr–1Mo (grade 91) type steels and austenitic alloys. The filler metal contains C and Cr levels that closely match those of the grade 91 steel in order to reduce the driving force associated with C migration, and the CTE at 540°C is nearly identical to that of the grade 91 steel. The filler metal is commercially identified as P87. Evaluation of the filler metal is in progress and preliminary mechanical property measurements have been reported.

Short term/high temperature strength data of all-weld metal and cross-weld samples for DMWs between grade 91 and 347H stainless steel made with filler metal P87 are shown in Fig. 35.[24] The yield strength of the all-weld metal samples (Fig. 35*a*) is higher than 347H stainless steel at temperatures considered and is only slightly below that of grade 91 steel at 480°C. The yield strength is above the grade 91 steel at higher temperatures. Similar results were observed with the tensile strength for both all-weld metal and cross-weld samples (Fig. 35*b*). Figure 36 shows creep rupture results in the form of a Larson–Miller parameter for welds made with various welding processes. The grade 91 average and (and 20% below average) values are also shown for reference. These results were generally conducted at elevated stresses and resulted in relatively short failure times. Failure locations for tests conducted at the higher stress levels were in the grade 91 base metal, while failures at the lower stress levels occurred in the fine grained region of the HAZ in the grade 91 material. Longer duration tests with estimated rupture lives of ~10 000 h are in progress[24] and appear to be needed to simulate the failure mechanism observed in the field. The results will also provide useful data for comparison to the performance of DMWs currently made with Inconel filler metals.

The fundamental cause of premature DMW failure is associated with gradients in both composition and CTE that exist across the fusion line. Thus, any long term solution to the problem should strive to minimise these gradients to the point where the adverse microstructural changes and localised stress concentrations are reduced to acceptable levels. One approach to this problem is to develop functionally graded transition joints in which the composition and concomitant properties are gradually varied in a controlled manner over relatively large distances. A schematic illustration of this concept is shown in Fig. 37. With this approach, the compositions at the ends of the transition joint match the ferritic steel and austenitic alloy, and the composition is varied gradually from one end of the joint to the other. The graded transition joint can then be inserted between the ferritic steel and austenitic alloy to permit the deposition of two similar welds at either end of the joint, replacing the single dissimilar weld that is prone to failure. This would eliminate the sharp changes in composition, microstructure and concomitant thermal and mechanical

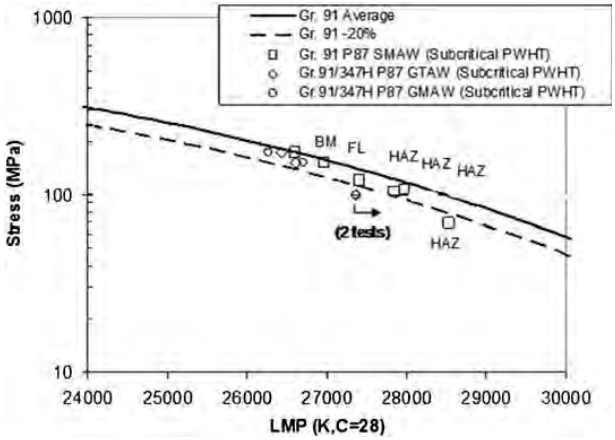

36 Creep rupture results in form of Larson–Miller parameter for welds made with P87 filler metal using various welding processes: grade 91 average and 20% below average values are also shown for reference

37 Schematic illustration of graded transition joint concept

ONLINE COLOUR ONLY

International Materials Reviews imr199.3d 28/3/12 16:43:10
The Charlesworth Group, Wakefield +44(0)1924 369598 - Rev 7.51n/W (Jan 20 2003)

ONLINE COLOUR ONLY

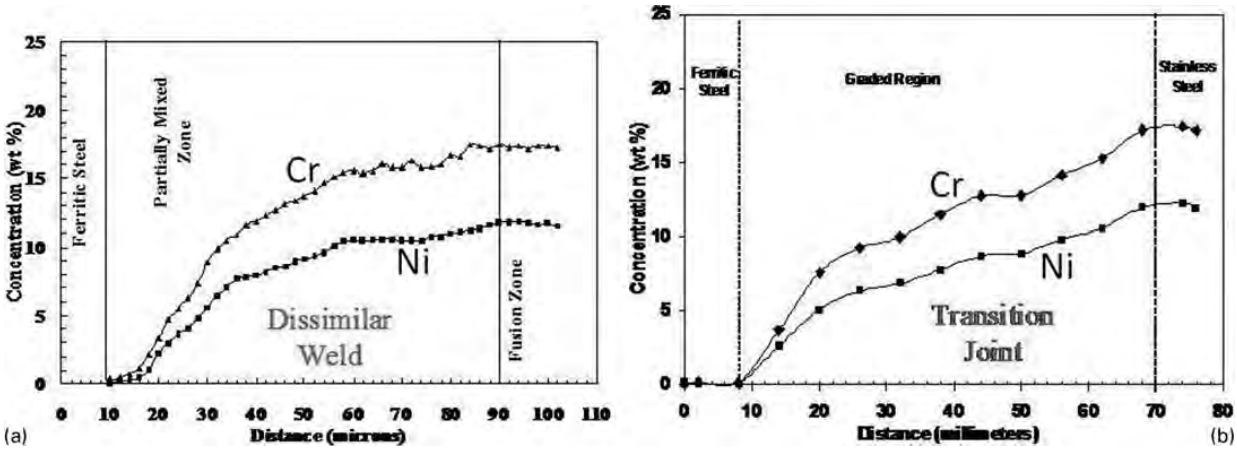

38 Comparison of Ni and Cr concentration gradients along *a* dissimilar weld and *b* transition joint between 1080 steel and 316 stainless steel produced with LENS process

properties, thus reducing or eliminating the DMW failure problem.

Research has recently been conducted to demonstrate the feasibility of this approach using the laser engineered net shaping (LENS) direct metal deposition process.[71] A transition joint between carbon steel and 316L stainless steel was fabricated with a 75 mm length, outer radius of 16 mm and wall thickness of 6 mm. These dimensions were chosen because they represent typical tube dimensions used by the power industry for waterwall panels in fossil fired boilers. The transition joint was fabricated by first depositing 12·5 mm of SAE 316L stainless steel onto an AISI 1080 steel substrate. Next, 50 mm of functionally graded material were deposited in which the SAE 316L composition changed gradually to AISI 1080 steel, and concluded with 12·5 mm of AISI 1080 steel. The 1080 steel and 316L stainless steel alloys were chosen because, at the time of fabrication, they were readily available and had the powder particle size range required for LENS processing. Microstructural characterisation results from this transition joint are described below. As described below, research is currently underway using more industrially relevant alloys.

The variation in Ni and Cr concentration along the transition joint described above is compared to that of a conventional DMW in Fig. 38. In the transition joint, the graded material between the ends varies gradually from 316L stainless steel to 1080 carbon steel. The concentration of all other alloying elements across the joint also varied in a smooth manner. The length of the composition gradient in the transition joint is ~60 mm, which is ~1000 times greater than the corresponding concentration gradient shown for the dissimilar metal weld (Fig. 38*a*), which is ~50 μm in length. The variation in microhardness across the joint is presented in Fig. 39. The extremities of the 316L and 1080 ends of the transition joint are noted in the figure. The hardness changes in a relatively smooth fashion with two notable exceptions. Local increases in hardness occur at the interface between the functionally graded material and the AISI 1080 end and the final layer of the 1080 steel. Microstructural characterisation showed that the first local increase in hardness was attributed to a mixed austenite/martensite microstructure. The second region of high hardness is attributed to as quenched martensite of the last layer of 1080 steel that is not tempered by the heating of subsequent layers. These high hardness regions occur due to the high carbon content of the 1080 powder that was used only for feasibility purposes. They can be minimised by the use of ferritic steels with lower C contents that are more representative of power plant steels.

Work is currently in progress to refine this technique for designing and fabricating graded transition joints

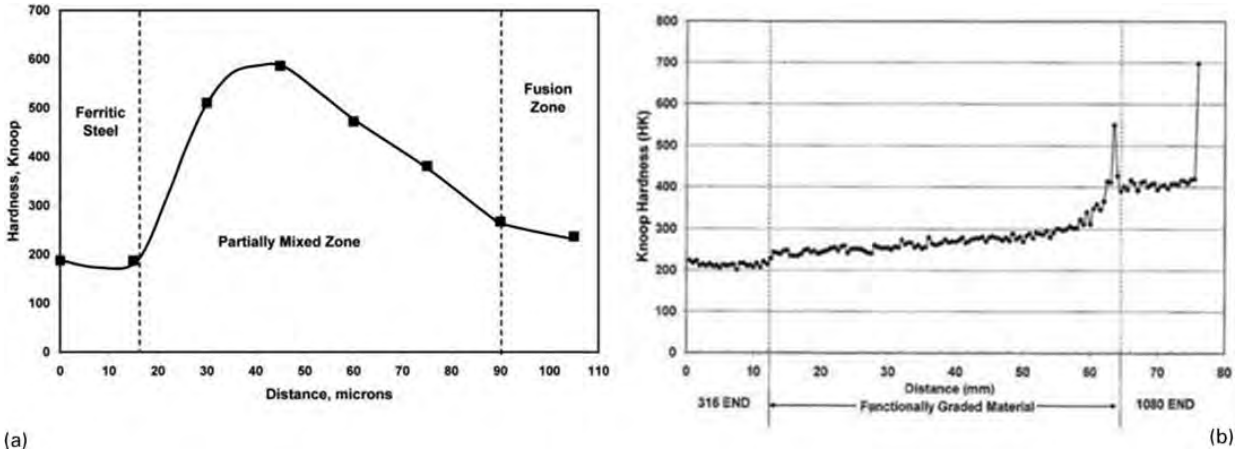

39 Comparison of hardness gradient along *a* dissimilar weld and *b* transition joint between 1080 steel and 316 stainless steel produced with LENS process

International Materials Reviews imr199.3d 28/3/12 16:43:20
The Charlesworth Group, Wakefield +44(0)1924 369598 - Rev 7.51n/W (Jan 20 2003)

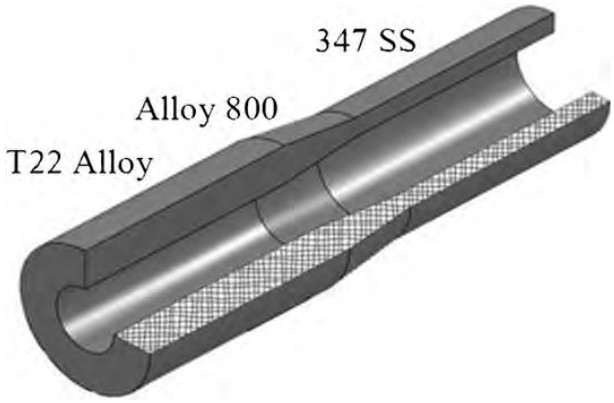

40 Conventional DMW joint design utilised for FE modelling

with optimal performance.[72] Thermodynamic and kinetic simulations are being used to identify the required length of the gradient needed to minimise the C migration problem, and FE calculations are used to estimate graded transition lengths that minimise stress concentrations due to CTE mismatch. Preliminary graded joints have been fabricated and utilised for microstructural and initial mechanical property characterisation.

Stress analysis was first conducted on a conventional DMW design commonly used in fossil fired power plants. These results served as a baseline in order to assess the effectiveness of graded transition joints for minimising stresses due to CTE mismatch. The DMW design is shown in Fig. 40. The joint is ~160 mm in length and joins a section of 2·25Cr–1Mo steel with 347H stainless steel using an interlayer of IN800. Finite element models of the conventional DMW and graded transition joints were created using the ANSYS FE software to determine the von Mises stress distribution in the joints. The joints were assumed to be stress free at 0°C. The stress distribution within the joints were simulated at an operating temperature of 650°C with a 20 000 N applied tensile load. The rotational symmetry allowed a two-dimensional model to be made for the three-dimensional geometry, and the hatch marked face in Fig. 40 shows the shape of the actual FE model. Stress distributions in the graded joints were determined by modelling the system as a layered structure in which the properties within each

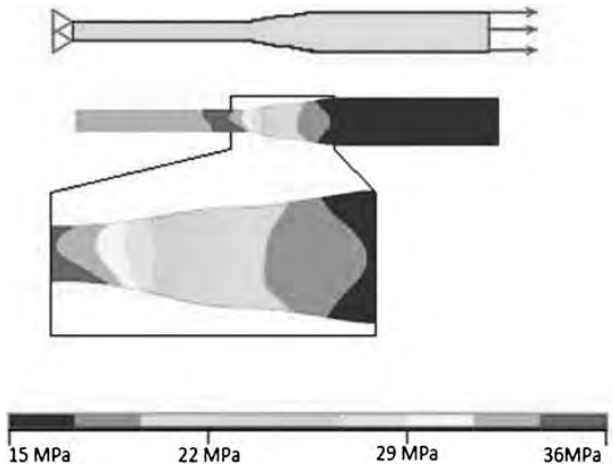

41 Results from simulation of uniform tube model with all T22 material showing von Mises stress distribution for 20 000 N applied tensile load at 650°C

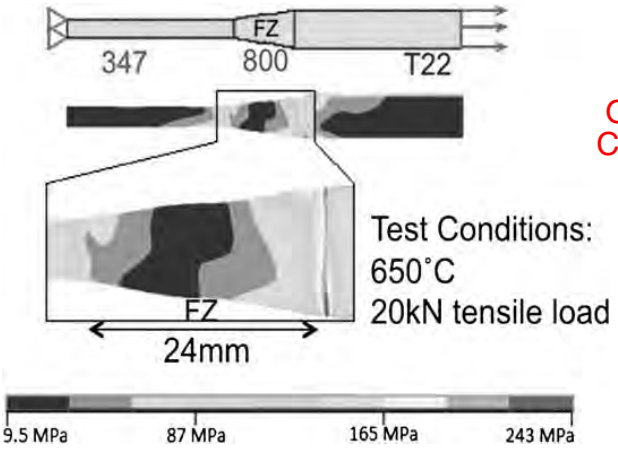

42 Results from original DMW joint model showing von Mises stress distribution with 20 000 N applied tensile load at 650°C

layer are constant, but vary continuously from layer to layer within the joint. A reduction of the layer width has the effect of smoothing out the mismatch in material properties and thus reducing the stress. This approach is justified based on the expected features of actual transition joints that have recently been fabricated[72] in which the composition (and therefore properties) of each layer within the joint are constant. This also provides a convenient method for stress minimisation by control of the layer width. An optimisation program was used to minimise the von Mises stress within the graded joints by adjusting the layer width and physical dimensions.

Figure 41 shows the von Mises stress distribution for a joint with dimensions shown for the DMW in Fig. 40, but with uniform material of 2·25Cr–1Mo steel. These results are useful for separating stress concentrations that arise due to changes in material properties and geometry across the joint. Here the maximum stress occurs in the thinner walled tube and is 36 MPa. This stress is slightly higher than the 32·4 MPa obtained by simply dividing the total load (20 000 N) by the cross sectional area of the thinner walled tube. The slight increase is due to the tapered geometry of the joint. Figure 42 shows the stress distribution in the DMW. Note that high von Mises stresses of ~240 MPa form immediately around the dissimilar material interfaces where failure is well known to occur. Figure 43 shows the stress distribution obtained when the load is increased to 20 000 N while holding the temperature fixed at 20°C, and Fig. 44 shows the opposite case in which the temperature is gradually increased to 650°C while no load is applied. The maximum stress is only ~33 MPa with the application of just the load. In contrast, the maximum stress due to CTE mismatch caused by the increase in temperature is nearly 240 MPa, which is similar to the effects from the combined load and temperature increase that was shown in Fig. 44. This result highlights the significance of CTE mismatch in producing high local stresses in DMWs.

Figure 45 shows the stress distribution for several graded transitions with various numbers of layers in the joint. The total length of the joint is fixed at 120 mm. Thus, the individual layer width is given simply by the total joint length (120 mm) divided by the number of layers in the joint. The maximum stress within the graded joint decreased significantly as the number of layers

ONLINE COLOUR ONLY

ONLINE COLOUR ONLY

International Materials Reviews imr199.3d 28/3/12 16:43:35
The Charlesworth Group, Wakefield +44(0)1924 369598 - Rev 7.51n/W (Jan 20 2003)

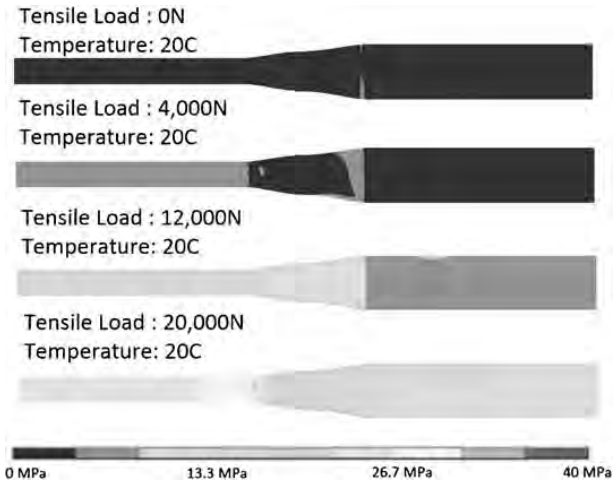

43 Results from simulation of original DMW joint shown with varying tensile loads (0, 4000, 12 000 and 20 000 N) applied at 20°C

increased. A stress reduction down to ~50 MPa was observed for a transition joint with 30 layers, which can be compared to the ~240 MPa level observed for the DMW joint exposed to the same conditions (650°C, 20 000 N tensile load). It was possible to provide further reductions in stress level down to ~40 MPa by locally increasing the wall thickness of the graded joint in high stress locations. This value is close to the materially homogenous joint (Fig. 41) of ~36 MPa.

Carbon diffusion as a function of time and temperature was modeled using DICTRA kinetic software.[73] The model used was similar to that described previously.[74,75] The composition, operating time and temperature were input as variables to determine the length of the graded region necessary to minimise carbon migration from a 2·25Cr–1Mo low alloy steel to IN800. This interface was modelled, because it exhibits the steepest C chemical potential gradient and is therefore most susceptible to carbon migration.

Figure 46*a* shows calculated carbon concentration profiles in the unaged condition, and after 2 and 20 years of service for the case in which the composition changes

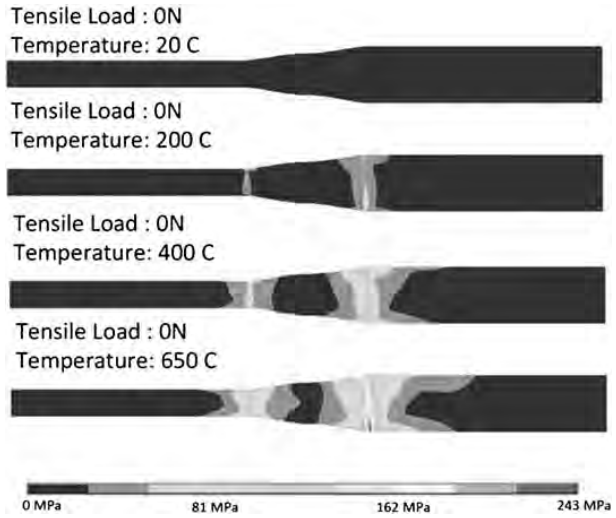

44 Results from simulation of original DMW joint shown at varying temperatures (20, 200, 400 and 650°C), with no tensile load applied

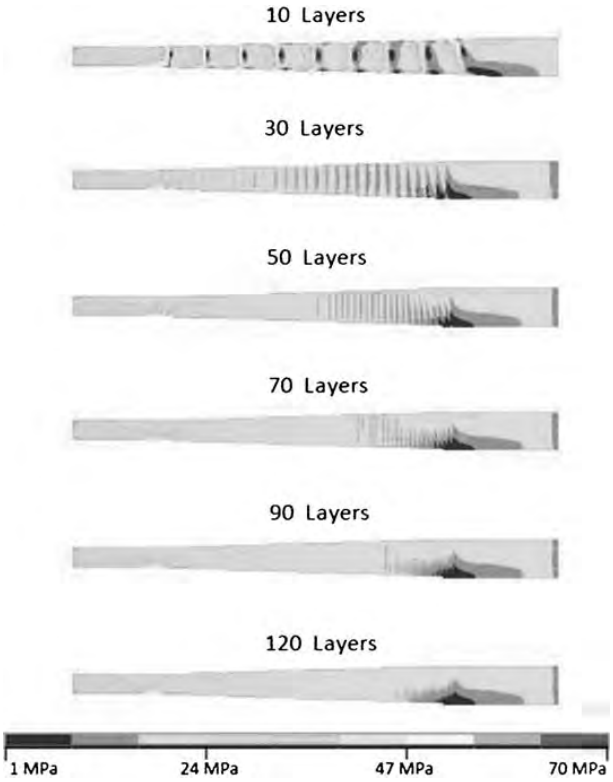

45 Results from FEA model of graded transition joint shown for varying number of grade layers with 20 000 N applied tensile load at 650°C

rather abruptly from 2·25Cr–1Mo to IN800 over a relatively short distance of 1 mm. Note that the carbon content in the 2·25Cr–1Mo steel drops from 0·12 to <0·04 wt-%, while there is a local increase near ~0·3 mm where the carbon concentration increases to ~0·135 wt-%. The location of the carbon peak corresponded to a peak in the $M_{23}C_6$ carbide content. These calculated results are consistent with those observed in practice, where a carbon depleted region forms in the ferritic material and a carbon enriched band of carbides forms along the fusion line in the austenitic material. Figure 46*b* and c show similar results in which the grade length is increased to 5 and 25 mm, respectively. The carbon migration problem is significantly reduced in the grade with a 25 mm length. This is attributed to the reduced carbon chemical potential that occurs with the larger grade length. The grade length required to minimise carbon migration will increase with increasing operating temperature due to an increase in carbon diffusivity. Figure 47 shows a summary of kinetic calculations, where the grade length required to reduce carbon migration to ten percent for a given temperature is shown. The results in this figure were obtained by repeating the calculations shown in Fig. 46 for temperatures between 500 and 650°C, and determining the grade length required to reduce carbon migration to ten percent for each temperature.

The modelling results described above provide useful insight into design requirements of graded transition joints. Research has been initiated to fabricate and test graded joints to verify the expected level of improvement. Fabrication was performed with a dual wire gas tungsten arc process in which the individual layer compositions within the joint are varied by simply adjusting the relative

ONLINE COLOUR ONLY
ONLINE COLOUR ONLY
ONLINE COLOUR ONLY

International Materials Reviews imr199.3d 28/3/12 16:43:44
The Charlesworth Group, Wakefield +44(0)1924 369598 - Rev 7.51n/W (Jan 20 2003)

ONLINE COLOUR ONLY

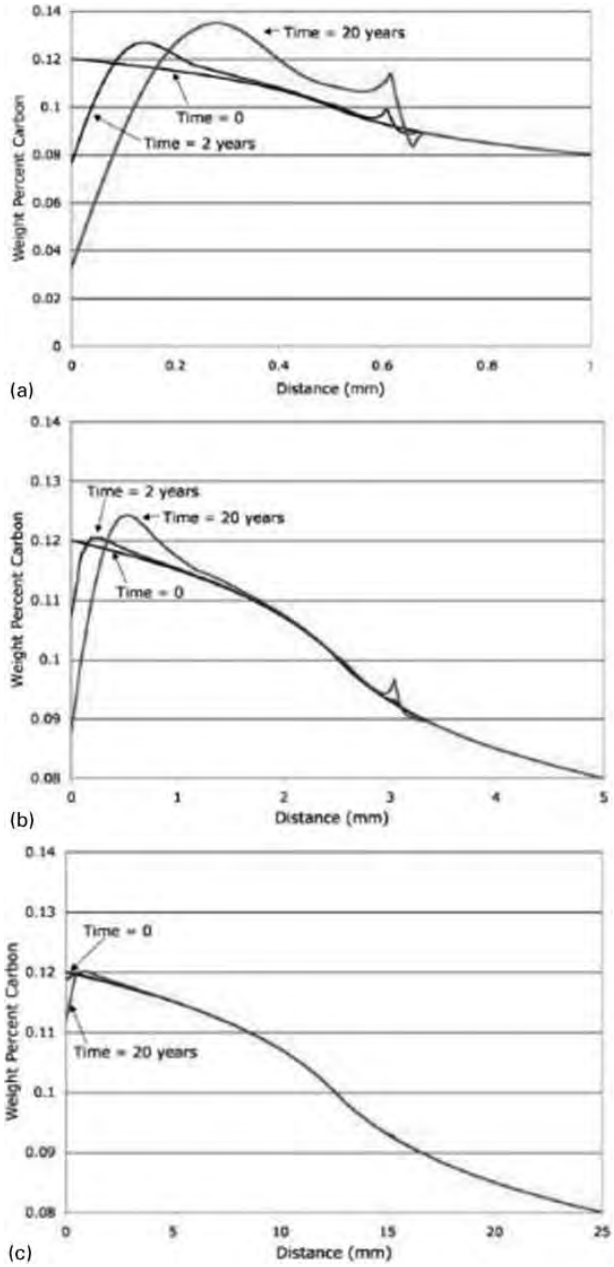

46 Predicted change in C concentration (calculated with DICTRA) at 500°C across joint between T22 and alloy 800 after 0, 2 and 20 years of simulated service for grade lengths of *a* 1 mm, *b* 5 mm and *c* 25 mm

filler metal feed rates of each alloy. This procedure eliminates some of the previous limitations encountered with the LENS process. The use of wire avoids the need for production of rather expensive powders associated with the LENS process. In addition, previous research has shown that only about 5–14% of the powder is actually deposited with the LENS process, with the remaining being wasted.[76] As a result, it is difficult to control the heat flow and deposit composition with powders, because the precise amount of powder that enters into the liquid pool is unknown. With wire filler metal, all of the material is fed directly into the melt pool and thus the composition can be more precisely controlled. This also permits higher deposition rates of $\sim$3 kg h^{-1}, compared to $\sim$0·2 kg h^{-1} with LENS process.

Figure 48 provides an example for a transition joint made between 2·25Cr–1Mo steel and alloy IN800. This

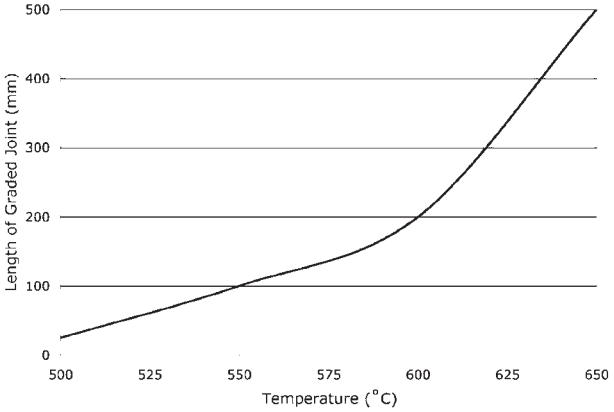

47 Predicted length of graded joint required to keep carbon migration below 10% after 20 years of simulated service for temperatures between 500 and 650°C

figure shows energy dispersive spectrometry measurements which reveal how the concentration of major alloying elements (Fe, Ni and Cr) varies across the transition joint. Note that the composition varies gradually from that of the 2·25Cr–1Mo steel to the IN800 over a distance of $\sim$50 mm. Also provided is the variation in microhardness along with the expected phase distribution within the joint. The predicted boundaries between the austenite and martensite regions were obtained by matching the measured nickel and chromium equivalents to the austenite and martensite phase boundaries on the Schaeffler diagram. There is a local increase in hardness between 20 and 30 mm that, according to the Schaeffler diagram, should correspond to the formation of martensite. This was verified through microstructural analysis. The local hardness peak is probably not desirable as it may lead to strain accumulation along the joint. The presence of martensite within the grade cannot be avoided,[6] due to the requirement of transitioning from ferrite to austenite from one end of the grade to the other. However, it should be possible to minimise this local hardness through a post-fabrication heat treatment. The hardness gradient in conventional DMWs occurs over $\sim$50 μm, which is a much higher hardness gradient than that shown in Fig. 48 that occurs over $\sim$5 mm. In addition, it is possible to reduce this hardness gradient further by simply reducing the composition gradient within the region where martensite forms. Long term testing is required to determine the potential effect of the hardness gradient on the creep behavioor.

The high temperature properties of graded transition joints must be established before use. Figure 49 shows the tensile properties of the 2·25Cr–1Mo/IN800 transition joint as a function of temperature. The minimum properties for the IN800 and 2·25Cr–1Mo steel are also shown for reference. The ductility and yield strength generally fall within the range for the end member alloys, while the tensile strength of the graded joint seems to follow the lower strength material at each temperature. In general, yielding followed by eventual fracture is expected to occur in the weakest region of the joint. However, there are other factors to consider when interpreting tensile data from graded materials. For example, the yield strength of the transition joint can be increased due to constraint of deformation in a soft region from a hard neighbouring region that restricts plastic flow. In addition, work hardening of any soft region can produce a

International Materials Reviews imr199.3d 28/3/12 16:43:52
The Charlesworth Group, Wakefield +44(0)1924 369598 - Rev 7.51n/W (Jan 20 2003)

ONLINE COLOUR ONLY

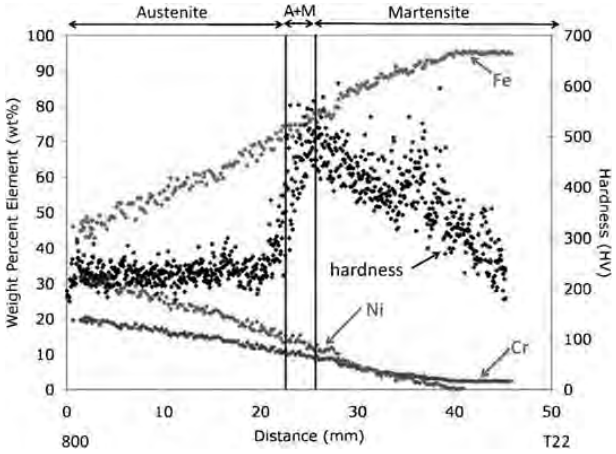

48 Variation in composition, microhardness and expected phase balance across 2·25Cr–1Mo/IN800 transition joint (A, austenite; M, martensite): '0' position refers IN800 to transition joint interface and '50 mm' position corresponds to location for 2·25Cr–1Mo steel

shift of the fracture from the region of initial deformation to another region. In any case, the results indicate that the transition joint should provide adequate short term tensile properties since the data generally fall within the range of wrought alloys that are used to make the grade. Creep testing is required to establish the long term behaviour of these joints relative to conventional DMWs and provide any insight for further optimisation that may be needed. Such tests are in progress and will be reported in the future.

Summary and future research

Microstructural evolution and premature failure of ferritic to austenitic DMWs have been reviewed. The microstructure of DMWs in the as welded condition consists of a sharp chemical concentration gradient across the fusion line that separates the ferritic and austenitic alloys. Upon cooling from the weld thermal cycle, a band of martensite forms within this concentration gradient due to high hardenability and the relatively rapid cooling rates associated with welding. Upon aging during PWHT and/or high temperature service, C diffuses down the chemical potential gradient from the ferritic steel toward the austenitic alloy. This can lead to formation of a soft C denuded zone near the interface in the ferritic steel, and nucleation and growth of carbides on the austenitic side that are associated with very high hardness. These large differences in microstructure and hardness occur over very short distances across the fusion line (about 50–100 μm). A band of carbides also forms along the fusion line in the ferritic side of the joint. The difference in hardness across the fusion line increases with increasing aging time due to nucleation and growth of the interfacial carbides.

Premature failure of DMWs is generally attributed to several primary factors, including: the sharp change in microstructure and mechanical properties across the fusion line, the large difference in CTE between the ferritic and austenitic alloys, formation of interfacial carbides that lead to creep cavity formation, and preferential oxidation of the ferritic steel near the fusion line. In general, the large gradient in mechanical properties and CTE serve to significantly concentrate the stress along the fusion line

ONLINE COLOUR ONLY

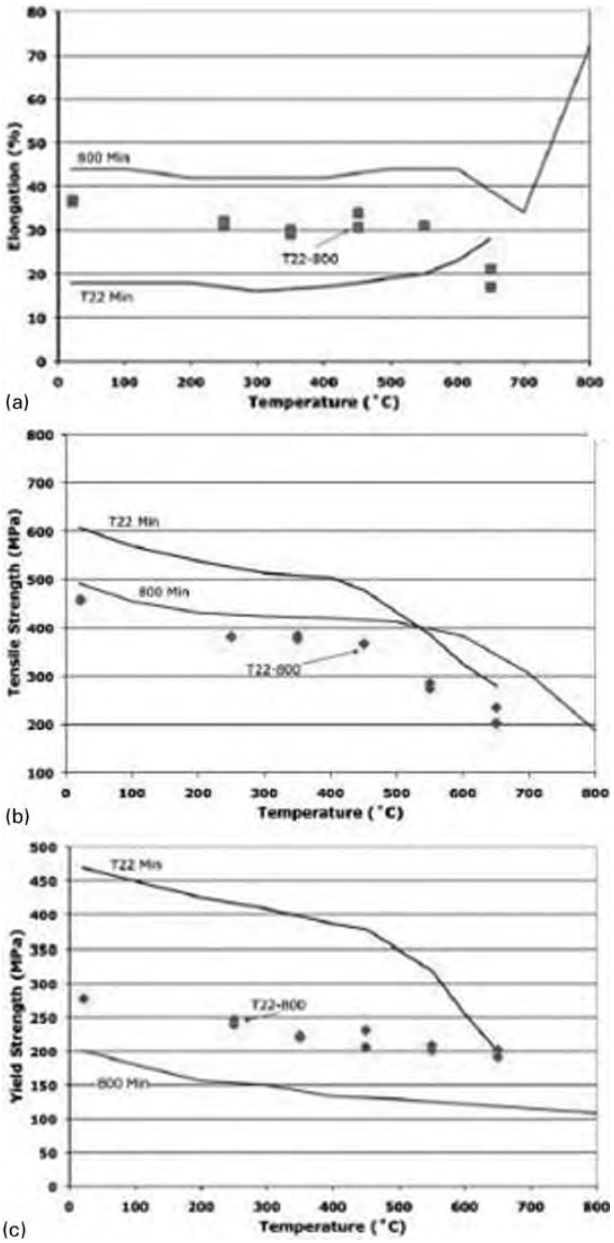

a elongation; *b* yield strength; *c* tensile strength

49 Tensile properties as function of temperature for graded transition joint between T22 and alloy 800: tensile tests were performed in air at strain rate of 0·005 min^{-1}; two samples were tested at each temperature; solid lines represent minimum nominal alloy data according to ASME code; data points are for transition joint

where a creep susceptible microstructure has evolved during aging. Presence of an oxide notch can concentrate the stress even further. Details of the failure mechanism and the relative importance of each factor varies. For DMWs made with Ni base filler metals, creep cavitation occurs in the ferritic steel along the row of carbides that form near the fusion line. For welds made with stainless steel filler metals, creep cavitation occurs along the PAGBs at a distance of about one to two grains from the fusion line. In thin walled tubing, the oxide notch can penetrate a relatively large fraction of the tube wall and play a major role in the failure. These mechanisms are not mutually exclusive, and mixed modes of failure can be observed.

International Materials Reviews imr199.3d 28/3/12 16:43:59
The Charlesworth Group, Wakefield +44(0)1924 369598 - Rev 7.51n/W (Jan 20 2003)

Current best practices for fabricating DMWs include the use of Ni base filler metals (to reduce C migration and CTE mismatch) and placement of welds in low temperature/low stress locations to the fullest extent permitted by design. Avoiding locations of aggressive environments that may accelerate the corrosion component of failure can also be effective. A variety of stress sources need to be considered, such as those from tube weight and steam pressure, in addition to stresses from through wall thermal gradients, temperature fluctuations, residual stresses from welding and mechanical restraint. Additional steps to prolong the life include the use of wide groove angles, reduction in geometrical changes across the weld joint and added weld reinforcement. The use of a PWHT does not appear to significantly affect the creep life of DMWs, and the heat treatment should be advantageous for reducing residual stress. Research is currently in progress to develop a new Ni base filler metal and graded transition joints for extending the life of DMWs.

Several areas warrant further research to provide a better understanding of the high temperature behaviour of DMWs and potentially improve performance. A larger creep rupture database would be helpful for more accurately establishing the long term service life, and any additional tests should be carefully designed to properly simulate the failure mechanism observed in the field. In particular, stress levels used for future creep tests should be below approximately 50–80 MPa in order to properly simulate field failures and provide data representative of service. Post-test characterisation of the creep samples is an important step in this effort to ensure the failure mechanism produced in the laboratory is representative of that observed in the field. The effect of gaseous impurities on the creep rupture behaviour should be established in more detail, especially for thin walled tubing applications in which corrosion can be an important component of failure. For applications in which environment may play an important role, investigations on the use of coatings may be warranted to improve service life. Long term creep tests that are supported by detailed post-test characterisation are needed for recently introduced P87 filler metal to confirm the expected improvement in performance for DMWs involving P91 type alloys. Similarly, the creep rupture behaviour of graded transition joints needs to be established relative to conventional DMWs. These results may also point to opportunities for improving the performance of transition joints by optimising the gradients in composition and associated properties within the joints. Modern modeling techniques should be combined with experimental results to guide this optimisation.

Acknowledgements

The author gratefully acknowledges the financial support provided for this work through the Next Generation Nuclear Plant Project, contract no. 93412, managed by Idaho National Laboratory (INL), which is supported by the US Department of Energy Office of Nuclear Energy under Department of Energy Idaho Operations Office contract no. DE-AC07-05ID14517. The author also appreciates the useful technical discussions with Ronald Mizia and Mike Patterson of INL. Review of the manuscript by Ronald Mizia, Gregory Brentrup and Brett Leister is also gratefully acknowledged.

References

1. R. Dooley and P. Chang: 'The current status of boiler tube failures in fossil plants', Proc. Int. Conf. on' Boiler tube failures in fossil plants', Nashville, TN, USA, November 1997, EPRI. 8
2. S. Sridhar, P. Rozzelle, B. Morreale and D. Alman: 'Materials challenges for advanced combustion and gasification fossil energy systems', *Metall. Mater. Trans.*, 2011, **42**, 871–877.
3. J. Collins, V. Tone and G. Gibbs: 'Next generation nuclear power plant project technology development roadmaps: the technical path forward for 750–800°C reactor outlet temperature', INL report no. EXT-09-16598, Idaho National Laboratory, Idaho Falls, ID, USA, 2009.
4. S. Kou: 'Welding metallurgy'; 2003, Hoboken, NJ, John Wiley and Sons Ltd.
5. K. Laha, K. S. Chandravathi, K. Bhanu Sankara Rao, S. L. Mannan and D. H. Sastry: 'An assessment of creep deformation and fracture behavior of 2·25Cr–1Mo similar and dissimilar weld joints', *Metall. Mater. Trans. A*, 2001, **32A**, 115–124.
6. J. DuPont and C. Kusko: 'Martensite formation in austenitic/ferritic dissimilar alloy welds', *Weld. J.*, 2007, **86**, 54S–57S.
7. S. Banovic, J. DuPont and A. Marder: 'Experimental evaluation of Fe–Al claddings in high temperature sulfidizing environments', *Weld. J.*, 2001, **80**, 62s–70s.
8. J. DuPont and A. Marder: 'Dilution in single pass arc welds', *Metall. Mater. Trans. B*, 1996, **27B**, 481–489.
9. M. Gittos and T. Gooch: 'The interface below stainless steel and nickel-alloy claddings', *Weld. J.*, 1992, **71**, 461s–472s.
10. A. Omar: 'Effects of welding parameters on hard zone formation at dissimilar metal welds', *Weld. J.*, 1998, **67**, 86s–93s.
11. C. D. Lundin: 'Dissimilar metal welds transition joints literature review', *Weld. J.*, 1982, **61**, 58s–63s.
12. G. Campbell, J. Elmer and W. Gibbs: 'Evaluation of factors controlling high temperature service life of 2–1/4Cr–1 Mo Steel to austenitic stainless steel weldments', In 'Trends in welding research in the United States', 443–470; 1981, Materials Park, OH, ASM.
13. J. Parker and G. Stratford: 'Review of factors affecting condition assessment of nickel based transition joints', *Sci. Technol. Weld. Join.*, 1999, **4**, 29–39.
14. J. D. Parker and G. C. Stratford: 'Characterization of microstructures in nickel based transition joints', *J. Mater. Sci.*, 2000, **35**, 4099–4107.
15. M. Sireesha, S. K. Albert and S. Sundaresan: 'Influence of high-temperature exposure on the microstructure and mechanical properties of dissimilar metal welds between modified 9Cr–1Mo steel and alloy 800', *Metall. Mater. Trans. A*, 2005, **36A**, 1495–1506.
16. S. K. Albert, T. P. S. Gill, A. K. Tyagi, S. L. Mannan and P. Rodrigues: 'Soft zone formation in dissimilar welds between two Cr–Mo steels', *Weld. J.*, 1997, **76**, 135s–142s.
17. R. Ryder*et al*: 'Dissimilar metal weld failures in power plants – causes and remedies', in 'Trends in electric utility research'; 1984, Chicagon, IL, Pergamon. 9
18. R. Christoffel and R. Curran: 'Carbon migration in welded joints at elevated temperatures', *Weld. J.*, 1956, **35**, 457s–468s.
19. T. Helander, J. Agren and J. Nilsson: 'An experimental and theoretical investigation of diffusion across a joint of two multi-component steels', *ISIJ Int.*, 1997, **37**, 1139–1145.
20. J. M. Race and H. Bhadeshia: 'Carbon migration across dissimilar steel welds', in 'International trends in welding science and technology', 1–5; 1993, Materials Park, OH, ASM.
21. B. Kim, H. An and J. Song: 'Analysis of carbon migration with post-weld heat treatment in dissimilar metal weld'in 'International trends in welding science and technology', 1–5; 1993, Materials Park, OH, ASM. 10
22. Y. You, R. K. Shiue, R. H. Shiue and C. Chen: 'The study of carbon migration in dissimilar welding of the modified 9Cr–1Mo steel', *J. Mater. Sci. Lett.*, 2001, **20**, 1429–1432.
23. J. F. Eckel: 'Diffusion across dissimilar metal joints', *Weld. J.*, 1964, **43**, 170s–178s.
24. J. Siefert, J. M. Sanders, J. M. Tanzosh, W. F. Newell, Jr and J. P. Shingledecker: 'Development of EPRI P87 solid wire', *Mater. High Temp.*, 2009, **27**, 243–252. 11
25. K. Coleman and D. Gandy: 'Alternative filler materials for DMWs involving P91 materials', in 'Advances in materials technology for fossil power plants', 940–967; 2008, Materials Park, OH, ASM.

International Materials Reviews imr199.3d 28/3/12 16:44:08
The Charlesworth Group, Wakefield +44(0)1924 369598 - Rev 7.51n/W (Jan 20 2003)

26. K. Yasuda: 'Cracking of overlay weldment for pressure vessel', Welding Research Committee of Japan Welding Society, 1982.
27. C. Li, R. Viswanathan and R. Ryder: 'Advances in life prediction methods'; 1983, New York, ASME.
28. R. David-Thomas, R. Diletto and J. DeLong: Proc. Conf. on 'Pressure vessels and piping', Minneapolis, MI, USA, June 1994, ASME, Vol. 288, 201.
29. B. Nath: 'Creep behaviour of dissimilar metal welds on stress relieving', Proc. 4th Int. Conf. on 'Welding in nuclear engineering', 52–56; 1982, Aachen, Deutschen Verband fur Schweibtechnik.
30. B. Nath: 'Creep rupture and creep crack growth behavior of transition joints', Proc. Int. Conf. on 'Welding technology for energy applications', 597–621; 1982, Gatlinburg, TN, Oak Ridge National Laboratory.
31. J. D. Parker and G. C. Stratford: 'The high-temperature performance of nickel-based transition joints: I. Deformation behavior', *Mater. Sci. Eng. A*, 2001, **A299**, 164–173.
32. J. D. Parker and G. C. Stratford: 'The high-temperature performance of nickel-based transition joints: II. Fracture behavior', *Mater. Sci. Eng. A*, 2001, **A299**, 174–184.
33. D. Roberts, R. Ryder and R. Viswanathan: 'Performance of dissimilar welds in service', *J. Press. Vess. Technol.*, 1985, **107**, 247–254.
34. R. Nicholson: 'Creep-rupture properties of austenitic and nickel-based transition joints', *Met. Technol.*, 1982, **9**, 305–311.
35. R. Nicholson: 'Effect of aging on interfacial structures of nickel-based transition joints', *Met. Technol.*, 1984, **11**, 115–124.
36. R. Viswanathan: Proc. Conf. on 'Boiler tube failures in fossil power plants', Palo Alto, CA, USA, November 1987, EPRI.
37. C. Wagner: 'Theory of precipitate aging via dissolution/reprecipitation: Ostwald ripening', *Z. Electrochem.*, 1961, **65**, 581.
38. I. Lifshitz: *J. Phys. Chem. Solids*, 1961, **19**, 35.
39. R. L. Klueh and J. F. King: 'Elevated-temperature tensile and creep-rupture behavior of alloy 800H/ERNiCr-3 weld metal/2·25Cr–1Mo steel dissimilar-metal weldments'; 1982, Oak Ridge, TN, Oak Ridge National Laboratory.
40. R. Nicholson and J. Williams: 'Failure and deformation modes in heavy section dissimilar welds subjected to accelerated thermal cycle: creep loading', *Int. J. Press. Vess. Pip.*, 1985, **20**, 239–274.
41. R. L. Klueh and J. F. King: 'Austenitic stainless steel–ferritic steel welded joint failures', *Weld. J.*, 1982, **61**, 302s–311s.
42. G. M. Slaughter and T. Housley: 'The welding of ferritic steels to austenitic stainless steels', *Weld. J.*, 1964, **43**, 454s–460s.
43. A. K. Bhaduri, S. Venkadesan, P. Rodriguez and P. G. Mukunda: 'Performance of a trimetallic transition joint', *Mater. High Temp.*, 1992, **10**, 45–50.
44. P. J. Budden and I. Curbishley: 'Assessment of creep crack growth in dissimilar metal welds', *Nucl. Eng. Des.*, 2000, **197**, 13–23.
45. J. A. Williams and J. D. Parker: 'Effect of thermal cycling on creep behavior of 2·25Cr–1Mo/type 316 steel dissimilar metal welds', *Mater. Sci. Technol.*, 1994, **10**, 915–923.
46. F. Gauzzi and S. Missori: 'Microstructural transformations in austenitic–ferritic transition joints', *J. Mater. Sci.*, 1988, **23**, 782–789.
47. R. Browne, B. J. Cane, J. D. Parker and D. J. Walters: 'Creep failure analysis of butt welded tubes', Proc. Int. Conf. on 'Creep and fracture of engineering materials and structures', Swansea, UK, March 1981, Pineridge Press, 645–657.
48. R. A. Ainsworth: 'Characterization of creep fracture at interfaces in weldments', in 'Recent advances in analytical fracture mechanics and fatigue', 143–153; 1997, Boston, MA, Kluwer Academic Publishers.
49. J. Tucker and F. Eberle: 'Development of a ferritic–austenitic weld joint for steam plant application', *Weld. J.*, 1956, **35**, 529S–540S.
50. R. W. Emerson, R. W. Jackson and C. A. Dauber: 'Transition joints between austenitic and ferritic steel piping for high temperature steam service', *Weld. J.*, 1962, **41**, 385–393.
51. J. D. Parker: 'High temperature failure of thick-section, low alloy steel to stainless steel transition weld', *Mater. High Temp.*, 1994, **12**, 25–33.
52. B. Roberts: 'Combustion engineering experience with dissimilar welds', Proc. Semin. on 'Dissimilar welds in fossil-fired boilers', Palo Alto, CA, USA, July 1985, EPRI, I73–I88.
53. J. F. King, M. D. Sullivan and G. M. Slaughter: 'Development of an improved stainless steel to ferritic steel transition joint', *Weld. J.*, 1977, **56**, 119–125.
54. W. Sartory: 'Revised analysis of the transition joint test'; 1984, Oak Ridge, TN, Oak Ridge National Laboratory.
55. D. Roberts, C. C. Li and R. D. Nicholson: in 'Dissimilar-weld failure analysis and development program', Vol. 8: 'Design and procedure guide for improved welds'; 1989, New York, EPRI.
56. E. Smith, B. Blanchard and R. Apps: in 'Welding of creep resistant steel', 79–89; 1970, Cambridge, The Welding Institute.
57. P. Roy and T. Lauritzen: 'The relative strength of base metal and heat-affected zone in 2·25Cr–1Mo weldments – a microstructural evaluation', *Weld. J.*, 1986, **65**, 45S–47S.
58. I. Chilton, A. Price and B. Wilshire: 'Creep deformation and local strain distributions in dissimilar metal welds between AISI type 316 and 2·25Cr–1Mo steels made with 17Cr–8Ni–2Mo weld metal', *Met. Technol.*, 1984, **11**, 383–391.
59. K. Laha, K. S. Chandravathi and K. B. S. Rao: 'Creep deformation and rupture behavior of 2·25Cr–1Mo steel weldments and its constituents (base metal, weld metal and simulated heat affected zones)', Proc. 2nd Int. Conf. on 'Heat resistant materials', Gatlinburg, TN, USA, September 1995, EPRI, 399–404.
60. R. Viswanathan and D. Gandy: 'A review of high temperature performance trends and design rules for Cr–Mo steel weldments'; 1998, Palo Alto, CA, EPRI.
61. R. L. Klueh and J. F. King: 'Thermal aging behavior of ERNiCr-3 alloy (weld and base metal)'; 1981, Oak Ridge, TN, Oak Ridge National Laboratory.
62. R. Klueh and J. King: 'Short-range order effects on the tensile behavior of a nickel-base alloy', *Metall. Mater. Trans. A*, 1979, **10A**, 1543–1548.
63. M. Sireesha, S. K. Albert and S. Sundaresan: 'Metallurgical changes and mechanical behavior during high temperature aging of welds between alloy 800 and 316LN austenitic stainless steel', *Mater. Sci. Technol.*, 2003, **19**, 1411–1417.
64. R. Viswanathan: 'Dissimilar metal weld and boiler creep damage evaluation for plant life extension', *J. Press. Vess. Technol.*, 1985, **107**, 218–225.
65. R. Ryder and C. Dahms: 'Design criteria for dissimilar metal welds'; 1990, New York, Welding Research Council.
66. J. D. Parker, T. Byrne and R. Dooley: 'Ontario hydro's experience with dissimilar metal welds in boiler tubing', Proc. Semin. on 'Dissimilar welds in fossil-fired boilers', New Orleans, LA, USA, February 1984, EPRI, 3-73–3-109.
67. R. Nicholson: 'Effect of post-weld heat treatment on development of interfacial structures in nickel-based transition joints', *Mater. Sci. Technol.*, 1985, **1**, 227–233.
68. W. Jones: 'Heat treatment effect on 2CrMo joints welded with a nickel-base electrode', *Weld. J.*, 1974, **53**, 225s–231s.
69. A. Joseph and S. K. Rai: 'Evaluation of residual stresses in dissimilar weld joints', *Int. J. Press. Vess. Pip.*, 2005, **82**, 700–705.
70. Proc. Semin. on 'Dissimilar welds in fossil-fired boilers', Palo Alto, CA, USA, July 1985, EPRI.
71. J. D. Farren, J. N. DuPont and F. Noecker: 'Fabrication of a carbon steel-to-stainless steel transition joint using direct laser deposition – a feasibility study', *Weld. J.*, 2007, **86**, 55S–61S.
72. G. Brentrup: MSc thesis, Lehigh University, Bethlehem, PA, USA, May 2011.
73. DICTRA, Thermo-Calc, Inc., Stockholm, Sweden.
74. A. Engström, L. Höglund and J. Ågren: 'Computer simulation of diffusion in multiphase systems', *Metall. Mater. Trans. A*, 1994, **25A**, 1127–1134.
75. T. Helander, J. Agren and J. Nilsson: 'An experimental and theoretical investigation of diffusion across a joint of two multicomponent Steels', *ISIJ Int.*, 1997, **37**, 1139–1145.
76. R. R. Unocic and J. N. DuPont: 'Process efficiency measurements in the laser engineered net shaping (LENS) process', *Metall. Mater. Trans. B*, 2003, **35B**, 143–152.

International Materials Reviews imr199.3d 28/3/12 16:44:09
The Charlesworth Group, Wakefield +44(0)1924 369598 - Rev 7.51n/W (Jan 20 2003)

Authors Queries

Journal: **International Materials Reviews**
Paper: **199**
Title: **Microstructural evolution and high temperature failure of ferritic to austenitic dissimilar welds**

Dear Author
During the preparation of your manuscript for publication, the questions listed below have arisen. Please attend to these matters and return this form with your proof. Many thanks for your assistance

Query Reference	Query	Remarks
1	Please provide 5–6 keywords.	
2	Please confirm the running head.	
3	This table has been supplied as an image rather than in an editable format. Please resupply in Word/Excel so that we can format the table into the journal style.	
4	Is this a ref. number?	
5	Ref. 17 does not correspond to the authors names 'Parker and Stratford' mentioned in this sentence, please check.	
6	Please confirm the change to figure caption 19.	
7	Please confirm the change to figure caption 31.	
8	Please provide the page/paper no.	
9	Please list all the authors' names and provide the page no.	
10	The page nos. of ref.20 and 21 are the same, please check.	
11	Please confirm the information supplemented.	
12	Please provide the page/paper no.	

13	Please confirm the info. supplemented to refs.47 and 48.	
14	Please confirm the info. supplemented to ref.52.	
15	Please provide the page no. and confirm the info. supplemented to ref.55.	
16	Please confirm the info. supplemented to ref.59.	
17	Please cite ref.60 in the text.	
18	Please provide the authors' names and page/paper no.	
19	Please provide the title of the thesis.	